International Journal of Plasticity 84 (2016) 1–32

Contents lists available at ScienceDirect

International Journal of Plasticity

journal homepage: www.elsevier.com/locate/ijplas

Phase field modeling of ductile fracture at finite strains: A variational gradient-extended plasticity-damage theory

Christian Miehe*, [1], Fadi Aldakheel, Arun Raina

Institute of Applied Mechanics (Civil Engineering), Chair I, University of Stuttgart, Pfaffenwaldring 7, 70569 Stuttgart, Germany

ARTICLE INFO

Article history:
Received 4 January 2016
Received in revised form 11 April 2016
Available online 26 April 2016

Keywords:
Phase field modeling
A. Crack Propagation and Arrest
B. Elastic-Viscoplastic Material
B. Finite Strain
C. Variational Calculus

ABSTRACT

This work outlines a rigorous variational-based framework for the phase field modeling of ductile fracture in elastic–plastic solids undergoing large strains. The phase field approach regularizes sharp crack surfaces within a pure continuum setting by a specific gradient damage modeling with geometric features rooted in fracture mechanics. It has proven immensely successful with regard to the analysis of complex crack topologies without the need for fracture-specific computational structure such as finite element design of crack discontinuities or intricate crack-tracking algorithms. Following the recent work Miehe et al. (2015), the phase field model of fracture is linked to a formulation of gradient plasticity at finite strains. The formulation includes two independent length scales which regularize both the plastic response as well as the crack discontinuities. This ensures that the damage zones of ductile fracture are inside of plastic zones, and guarantees on the computational side a mesh objectivity in post-critical ranges. The novel aspect of this work is a precise representation of this framework in a canonical format governed by variational principles. The coupling of gradient plasticity to gradient damage is realized by a constitutive work density function that includes the stored elastic energy and the dissipated work due to plasticity and fracture. The latter represents a coupled resistance to plasticity and damage, depending on the gradient-extended internal variables which enter plastic yield functions and fracture threshold functions. With this viewpoint on the generalized internal variables at hand, the thermodynamic formulation is outlined for gradient-extended dissipative solids with generalized internal variables which are passive in nature. It is specified for a conceptual model of von Mises-type elasto-plasticity at finite strains coupled with fracture. The canonical theory proposed is shown to be governed by a rate-type minimization principle, which fully determines the coupled multi-field evolution problem. This is exploited on the numerical side by a fully symmetric monolithic finite element implementation. The performance of the formulation is demonstrated by means of some representative examples.

1. Introduction

Fracture in the form of evolving crack surfaces in ductile solid materials is preceded by significant plastic distortion. The prediction of failure mechanisms due to crack initiation and growth coupled with elastic–plastic deformations is an

* Corresponding author. Tel.: +49 711 685 66379.
E-mail address: cm@mechbau.uni-stuttgart.de (C. Miehe).
[1] URL: www.mechbau.uni-stuttgart.de/ls1/.

http://dx.doi.org/10.1016/j.ijplas.2016.04.011
0749-6419/

intriguingly challenging task, and plays an extremely important role in various engineering applications. This covers machining, cutting and forming of ductile metals and polymers, i.e. applications at the core of automobile, aerospace or heavy industries which significantly benefit from precisely predictive computational tools to model ductile fracture in the design phase of products. To this end, a rigorous variational-based framework is presented for an innovative phase field modeling of ductile fracture in elastic–plastic solids undergoing large strains.

1.1. Plasticity, damage and fracture in ductile materials

Ductile fracture is a phenomenon that couples at the macroscopic level *plastic deformations* with the *accumulation of damage* and *crack propagation*. The process of damage that follows extensive plastic deformations covers the macroscopic effects of degrading stiffness, strength and ductility up to a critical state where rupture occurs. Damage is caused by deformation mechanisms at the microscopic level, such as void nucleation, growth and coalescence, the formation of micro-shear-bands and micro-cracks. A great number of pure phenomenological and micro-mechanically motivated approaches exists for the continuum modeling of ductile fracture, see for example Besson (2010) and Li et al. (2011) for overviews. The simplest approaches provide *estimates* for the local initiation of fracture *uncoupled* from the plastic deformation, for example by introducing a damage field variable that counts towards the local initiation of fracture, see Johnson and Cook (1985). In contrast, *coupled formulations* link the evolution of damage to the evolution of plastic deformation. This covers on the one side the pure phenomenological macro-models of *continuum damage mechanics*, see for example Lemaitre (1985) and Lemaitre and Chaboche (1990). On the other side, models of *porous plasticity* describe micro-mechanical mechanisms such as void growth, and obtain macroscopic constitutive expressions by analytical homogenization techniques. This includes early investigations such as Rice and Tracey (1969) on exponential growth of voids in an ideal plastic matrix under remote strain action. Gurson (1975) obtained a macroscopic yield surface by homogenization of a porous RVE with assumed rigid plastic flow, that degrades with increasing void fraction. It was enhanced by Needleman and Tvergaard (1984) and many follow-up works to include effects of void nucleation and coalescence. Alternative homogenization-based models for porous plasticity are suggested for example in Ponte Castañeda and Zaidman (1994) and Leblond et al. (1994). There is a constantly evolving vast literature on improved damage models for porous materials, see for example Nahshon and Hutchinson (2008), Danas and Ponte Castañeda (2012) and Khan and Liu (2012), Brünig et al. (2013) for recent contributions.

However, in these *local models* of plasticity coupled with damage, the strong softening behavior induces *localization* of plastic and damage zones. The accompanying loss of ellipticity or hyperbolicity in quasi-static or dynamic cases results in the pathological mesh dependence of finite element implementations, where localized zones are determined by the element size of spatial discretizations. A way to overcome this problem is the construction of *gradient plasticity* and *gradient damage* models which *limit the width* of localized plastic and damage zones due to their inherent *length scales* and *size effects* of the dissipative response. On the side of plasticity theory, gradient-enhanced models are naturally rooted in micro-mechanical descriptions of dislocation flow in crystals, where the *plastic length scale* is related to the lattice spacing, see Nye (1953), Kröner (1960) and Fleck and Hutchinson (1997). Associated models of single crystal gradient-plasticity are proposed by many authors, e.g. Gurtin (2002), Svendsen (2002) and Evers et al. (2004), see also the recent overviews in Clayton (2011) and Steinmann (2015). In contrast, pure phenomenologically-based theories of gradient plasticity often use plastic length scales as limiters of localized zones determined by macroscopic experiments, see for example Mühlhaus and Aifantis (1991), Geers (2004) and Reddy et al. (2008). Recently Miehe (2011, 2014) proposed a unified framework of strain-gradient plasticity based on multi-field variational principles for both geometrically linear and non-linear setting. On the side of damage mechanics, formulations of gradient-enhanced models are mostly applied to the modeling of degradation effects in brittle or quasi-brittle materials, see for example Peerlings et al. (1996), Frémond and Nedjar (1996) and Comi (1999). Here, a *damage length scale* that limits localized zones is introduced, determined by macroscopic experiments. The recent works Miehe et al. (2010a) and Pham et al. (2011) apply gradient damage models to the regularized description of Griffith-type brittle fracture. The coupling of *local* plasticity with gradient-damage models have already been used extensively to model ductile fracture, see for example de Borst et al. (1999), Nedjar (2001), Reusch et al. (2003), Alessi et al. (2015) and Ambati et al. (2015). However, mesh objective response of these models in post-critical ranges cannot be established due to the missing *plastic length scale* and inherent nature of local plastic strains. Furthermore, as noted by Alessi et al. (2015), a model of gradient damage coupled with plasticity allows the *nucleation of cohesive cracks*, i.e. the existence of a surface of discontinuity of displacements with non-vanishing stress. These constraints can only be achieved by defining length scales and limiters for *both* the plastic as well as the damage zones with a distinct relationship, such that a localized *damage zone develops inside of a localized plastic zone*. Recent works in this direction are Aslan et al. (2011), Dimitrijevic and Hackl (2011), Saanouni and Hamed (2013) and Miehe et al. (2015). In this work, we develop a rigorous variational foundation for the coupling of gradient plasticity to gradient damage models at finite strains.

Most of the above mentioned continuum approaches to the modeling of strain softening are not able to model the basic ingredient of fracture, i.e. *sharp crack discontinuities and their propagation* which succeed the damage evolution. In the computational modeling, this needs in addition a formulation of surfaces which evolve in the solid, driven by configurational forces. There exists a large body of references in the computational literature for the modeling of strong discontinuities by *cohesive zone models*, allowing the description of sharp cracks by introducing displacement jumps in the kinematical description. Simo et al. (1993), Oliver (1996a,b) and Linder and Raina (2013) embed discontinuities in finite *elements*. Xu and

Needleman (1994), Ortiz and Pandolfi (1999) and Miehe and Gürses (2007) formulate discontinuities on *interfaces* between finite elements. Belytschko and Black (1999), Moës et al. (1999), Wells and Sluys (2001) use *nodal-enrichment strategies*. The coupling of porous plasticity with cohesive zone type sharp crack discontinuities to model ductile fracture was considered in Huespe et al. (2009, 2012) based on element and Crete et al. (2014) based on nodal enrichments. However, this tracking of sharp crack surfaces provides substantial difficulties in numerical implementations and often restricts the above formulations to simple crack topologies.

1.2. Variational phase field modeling of ductile fracture

This can be overcome by recently developed phase field approaches to fracture, which regularize sharp crack discontinuities within a pure continuum formulation. This *diffusive* crack modeling allows the resolution of complex failure topologies, such as crack branching phenomena in dynamic fracture of brittle solids, see Hofacker and Miehe (2012) and references cited therein. In contrast to computational models which model sharp cracks, the phase field approach is a spatially smooth continuum formulation that avoids the modeling of discontinuities and can be implemented in a straightforward manner by coupled multi-field finite element solvers. Three basic approaches to the regularized modeling of Griffith-type *brittle fracture* in elastic solids may be distinguished: (i) The phase field approach by Karma et al. (2001) and Hakim and Karma (2009) apply a Ginzburg-Landau-type evolution of an unconstrained crack phase field, using a non-convex degradation function that separates unbroken and broken states. It *lacks explicit definitions of irreversibility constraints* for the crack evolution. (ii) The approach of Francfort and Marigo (1998), Bourdin et al. (2000, 2008), adopts the variational structure and Γ-convergent regularization of image segmentation developed by Mumford and Shah (1989) and Ambrosio and Tortorelli (1990) for the analysis of finite increments in quasi-static crack evolution. The irreversibility of the fracture process is modeled by *evolving Dirichlet-type boundary conditions*, while the scalar auxiliary field used for the regularization is un-constrained. This needs the implementation of a non-standard code structures in typical finite element solvers. The phase field approach by Miehe et al. (2010a,b) is a gradient damage theory with a *local irreversibility constraint* on the crack phase field, however, equipped with constitutive structures rooted in fracture mechanics. It incorporates regularized crack surface density functions as central constitutive objects, which is motivated in a descriptive format based on geometric considerations. Such a formulation can easily be implemented by a multi-field finite element solver with monolithic or staggered solution of the coupled problem. Recent works on brittle fracture along this third line are Pham et al. (2011), Borden et al. (2012) and Verhoosel and de Borst (2013).

Extensions to the phase field modeling of ductile fracture are exclusively related to the third line, representing conceptually a coupling of gradient damage mechanics with models of elasto-plasticity. Duda et al. (2014) investigates a setting of brittle fracture in elastic–plastic solids. Variational-based approaches to combined brittle-ductile fracture are outlined in Ulmer et al. (2013) and Alessi et al. (2015). The model suggested in Ambati et al. (2015) uses a characteristic degradation function that couples damage to plasticity in a multiplicative format. However, these settings combine *local models* of plasticity to the gradient-damage-type phase field modeling of fracture and do not meet the demands mentioned above, i.e. related plastic and damage length scales. Furthermore, settings outlined in Ambati et al. (2015) lack a canonical structure based on variational principles. This is achieved in recent work Miehe et al. (2015) that couples gradient plasticity to gradient damage at finite strains.

This paper is to present a consistent variational-based framework for the phase field modeling of ductile fracture in elastic–plastic solids undergoing large strains. It links a formulation of *variational gradient plasticity*, as recently outlined in Miehe (2011, 2014), to a specific setting of *variational gradient damage*, rooted in the phase field approach of fracture suggested by Miehe et al. (2010a,b). Such a formulation has conceptually been outlined in Miehe et al. (2015) and is recast in this work into a canonical variational formulation. The basic ingredients of formulation proposed here are:

- A phase field model for ductile fracture that combines ingredients of gradient plasticity and gradient damage, offering a *scaling of plastic to damage length scales.*
- A thermodynamic framework that is fully variational in nature, based on a split of a *work density function* into energetic and dissipative parts, and a *dissipation function* with separate thresholds for plasticity and damage.

The approach is embedded in the theory of *gradient-extended continuum modeling*, as outlined in the general context by Maugin (1990), Capriz (1989), Mariano (2001) and Frémond (2002). The gradient plasticity-damage coupling is conceptually based on a *work density function* that governs the rate-independent part of a solid undergoing elastic–plastic deformations at fracture. It assumes a *phase transition* of the elastic–plastic work density towards a given critical value, that provides locally a *threshold for brittle or ductile fracture*. The constitutive structure of the work density function includes in a modular format separate constitutive functions with a clear physical meaning. On the side of the elastic–plastic bulk response, this covers the *elastic work density function* and the *plastic work density function* of an undamaged material. On the side of regularized fracture mechanics, a *crack surface density function* is introduced that can be geometrically motivated by a regularization of a sharp crack. Finally, the elastic-plastic-damage coupling is governed by a *degradation function*, that is assumed to be convex in nature as used previously in damage mechanics. For this canonically simple model, the coupling of gradient plasticity and gradient damage is realized by only two material parameters: a critical elastic–plastic

work density w_c that governs the onset of fracture and a parameter ζ that controls the shape of the post-critical range of damage.

A further split of the work density function into an energetic part that is stored and a dissipative part provides the thermodynamic foundation of the model. Here, the energetic part is defined to be exclusively elastic in nature, representing a degraded elastic free energy density. Besides the constitutive expression for the stresses, it provides locally *energetic driving forces* of plasticity as well as regularized fracture. The dissipative part governs *plastic and fracture resistances*, each equipped with length scales l_p and l_f, which includes the coupling between gradient plasticity and gradient damage. This viewpoint settles the general *framework of gradient extended modeling*. The variables responsible for the length scale effects are the equivalent plastic strain and the fracture phase field. They are considered to be *passive in nature*, i.e. governed by Dirichlet and Neumann-type boundary conditions which do not allow an independent load-type driving. Hence, micro-balance-type theories such as considered in full generality by Gurtin (1996, 2003) or Forest (2009) are avoided in this setting. Due to the specific split of the work density function into energetic and dissipative part, the *dissipation is defined fully local in nature*. This allows a decomposition into plastic and fracture parts, defining separate energetic driving forces for the evolution of plastic deformation and the accumulation of fracture. A numerical integration of these separate plastic and fracture contributions to the dissipation then allows a decomposition of the dissipative part of the work density function into contributions due to plasticity and fracture.

This decomposition of the dissipation into plastic and fracture parts offers a clear structure for the constitutive modeling of the evolution equations. Here, a formulation is constructed based on *two separate threshold functions for plasticity and fracture*, each driven by the driving forces which govern the dissipation due to plasticity and fracture. The associated resistances are defined by variational derivatives of the dissipative part of the work density function. As a conceptual example, we consider a von-Mises-type plastic flow with gradient-enhanced hardening, and a scalar function for the fracture threshold. With these two additional threshold functions at hand, a *dissipation potential function* is constructed that additively splits into plastic and regularized fracture parts. It is shown that the coupled plasticity-damage model is thermodynamically consistent. A detailed analysis comments on the role of the material parameters and points out for a one-dimensional problem the characteristics of the modeling concept. The approach models both brittle as well as ductile fracture. The occurrence and sequence of these phenomena depends on the choice of the material parameters.

The proposed structure is shown to be fully variational in nature. To this end, a *rate-type minimization problem* is developed for the quasi-static case that neglects inertia effects. The variational nature of the problem provides a fully symmetric setting of the multi-field problem. This is in contrast to traditional formulations of coupled plasticity-damage models, such as considered by Lemaitre (1985) and the recent phase field formulation outlined in Ambati et al. (2015). The structure of the evolution equation for the two scalar internal variables, i.e. the equivalent plastic strain and the fracture phase field, is analyzed and shown to have a formally similar structure. In particular, we consider possible modifications of the phase field equation accounting for fracture in tension. Finally, the modeling performance of the formulation is underlined by characteristic benchmark problems. Here, the need of the coupling of gradient plasticity–damage is highlighted, that is needed to obtain a mesh-objective post-critical response as well as physically reasonable results with regard to the diffuse distribution of localized plastic strains and damage.

2. Introduction of primary field variables

2.1. Finite gradient plasticity in the logarithmic strain space

2.1.1. Finite deformations

Let $\boldsymbol{\varphi}(\boldsymbol{X},t)$ with initial condition $\boldsymbol{\varphi}(\boldsymbol{X},t_0)=\boldsymbol{X}$ be the deformation map at time t that maps material positions $\boldsymbol{X}\in\mathscr{B}_0$ of the reference configuration $\mathscr{B}_0\in\mathscr{R}^3$ onto points $\boldsymbol{x}=\boldsymbol{\varphi}_t(\boldsymbol{X})\in\mathscr{B}_t$ of the current configuration $\mathscr{B}_t\in\mathscr{R}^3$ as visualized in Fig. 1. The material deformation gradient is defined by $\boldsymbol{F}:=\nabla\boldsymbol{\varphi}_t(\boldsymbol{X})$ with $\det[\boldsymbol{F}]>0$. The solid is loaded by prescribed deformations and external traction on the boundary, defined by time-dependent ("active") Dirichlet- and Neumann-conditions

$$\boldsymbol{\varphi}=\overline{\boldsymbol{\varphi}}(\boldsymbol{X},t) \text{ on } \partial\mathscr{B}_0^{\varphi} \quad \text{and} \quad \boldsymbol{P}\boldsymbol{n}_0=\bar{\boldsymbol{t}}_0(\boldsymbol{X},t) \text{ on } \partial\mathscr{B}_0^{t} \tag{1}$$

on the surface $\partial\mathscr{B}_0=\partial\mathscr{B}_0^{\varphi}\cup\partial\mathscr{B}_0^{t}$ of the undeformed configuration. The first Piola stress tensor $\boldsymbol{P}$ is the thermodynamic dual to $\boldsymbol{F}$.

2.1.2. Definition of an elastic strain measure

Following (Miehe, 1998; Miehe et al., 2002), we focus on a phenomenological setting of finite plasticity based on an additive decomposition of a *Lagrangian Hencky strain* $\boldsymbol{\varepsilon}$ with coordinates ε_{AB}. This allows to defines a stress producing elastic strain measure

$$\boldsymbol{\varepsilon}^e:=\boldsymbol{\varepsilon}-\boldsymbol{\varepsilon}^p \quad \text{with} \quad \boldsymbol{\varepsilon}:=\frac{1}{2}\ln\boldsymbol{C} \quad \text{and} \quad \boldsymbol{C}:=\boldsymbol{F}^T\boldsymbol{g}\boldsymbol{F}, \tag{2}$$

where $\boldsymbol{C}$ with coordinates $C_{AB}=g_{ab}F^a_AF^b_B$ is the right Cauchy-Green tensor, i.e. the representation of the Eulerian standard metric $\boldsymbol{g}$ in the reference configuration. The *logarithmic plastic strain* $\boldsymbol{\varepsilon}^p(\boldsymbol{X},t)$ with coordinates ε^p_{AB} is a local internal variable,

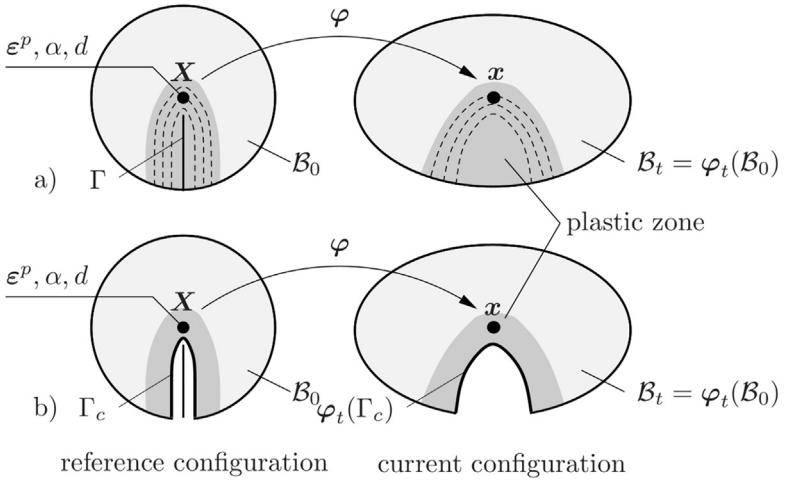

Fig. 1. Finite deformation of a solid with a regularized crack *inside* of a plastic zone. The *deformation map* $\boldsymbol{\varphi}$ maps at time t the reference configuration $\mathscr{B}_0$ onto the current configuration $\mathscr{B}_t$. a) The *crack phase field* $d \in [0,1]$ defines a regularized crack surface functional $\Gamma_l(d)$ that converges in the limit $l_f \to 0$ to the sharp crack surface Γ. b) The level set $\Gamma_c = \{\boldsymbol{X} | d = c\}$ defines for a constant $c \approx 1$ the crack faces in the regularized setting. Parts of the continuum with $d > c$ are considered to be free space and are not displayed.

related by $\boldsymbol{\varepsilon}^p = \tfrac{1}{2}\ln \boldsymbol{G}^p$ to a plastic metric $\boldsymbol{G}^p \in Sym_+(3)$. It starts to evolve from the initial condition $\boldsymbol{\varepsilon}^p(\boldsymbol{X},t_0)=0$. The additive decomposition (2) in the logarithmic strain space allows for a simple extension of constitutive structures for the geometrically linear setting to the nonlinear case. Note that $\boldsymbol{\varepsilon}^e$ is a priori an objective variable due to its Lagrangian nature.

2.1.3. Isotropic strain-gradient plasticity

We consider a framework of isotropic finite gradient plasticity at fracture. To this end, a scalar *isotropic hardening variable* $\alpha(\boldsymbol{X},t)$ is introduced, that defines an equivalent plastic strain in the logarithmic strain space by the evolution equation

$$\dot{\alpha} = \sqrt{\frac{2}{3}} \|\dot{\boldsymbol{\varepsilon}}^p\| \quad \text{with} \quad \dot{\alpha} \geq 0. \tag{3}$$

It starts to evolve from the initial condition $\alpha(\boldsymbol{X},t_0)=0$. In the subsequent treatment, we introduce the *plastic length scale* l_p that accounts for size effects to overcome the non-physical mesh sensitivity in ductile fracture. To this end, we focus on a first order setting of gradient plasticity where the gradient $\nabla\alpha(\boldsymbol{X},t)$ enters the constitutive functions. The generalized internal variable field α is considered as passive in the sense that an external driving is not allowed. This is consistent with the time-independent ("passive") Dirichlet- and Neumann conditions

$$\alpha = 0 \text{ on } \partial\mathscr{B}_0^{\alpha} \quad \text{and} \quad \nabla\alpha \cdot \boldsymbol{n}_0 = 0 \text{ on } \partial\mathscr{B}_0^{\nabla\alpha} \tag{4}$$

on the surface $\partial\mathscr{B}_0 = \partial\mathscr{B}_0^{\alpha} \cup \partial\mathscr{B}_0^{\nabla\alpha}$ of the undeformed configuration, defining "micro-clamped" and "free" constraints for the evolution of the plastic deformation.

2.2. The phase field approximation of sharp cracks

Following previous treatments Miehe et al. (2010a), we consider the phase field approach to fracture as a specific formulation of gradient damage mechanics. It is based on a geometric regularization of sharp crack discontinuities that is governed by a *crack phase field*

$$d \in [0,1] \quad \text{with} \quad \dot{d} \geq 0 \tag{5}$$

as indicated in Fig. 2. It characterizes locally for the initial condition $d(\boldsymbol{X},t)=0$ the unbroken and for $d(\boldsymbol{X},t)=1$ the fully broken state of the material. In contrast to traditional approaches to gradient damage mechanics, the crack phase field d is considered to have a purely geometric meaning. It governs the *regularized crack surface*

$$\Gamma_l(d) = \int_{\mathscr{B}_0} \widehat{\gamma}(d, \nabla d)\, dV \quad \text{with} \quad \widehat{\gamma}(d, \nabla d) = \frac{1}{2l_f} d^2 + \frac{l_f}{2} \left|\nabla d\right|^2 \tag{6}$$

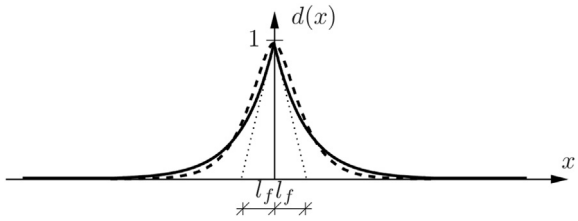

Fig. 2. Diffusive crack modeling at $x=0$ modeled with the length scale $l_f \leq l_p$. Regularized curves obtained from minimization principle of diffusive crack topoloy $\int_{\mathscr{B}_0} \gamma_l \mathrm{dV} \to \min$ with crack surface density function γ_l. Thick line: $\gamma_l = d^2/2l_f + l_f|\nabla d|^2/2$ with regularization profile $exp[-|x|/l_f]$ satisfying $d(0)=1$, dotted line: $\gamma_l = \mathrm{d}^2/2l_f + l_f\left|\nabla d\right|^2/4 + l_f^3(\Delta d)^2/32$ with regularization profile $exp[-2|x|/l_f](1+2|x|/l_f)$ satisfying $d(0)=1$ and $d'(0)=0$.

that is formulated in terms of an isotropic *crack surface density function* per unit volume of the solid. The regularization is governed by a *fracture length scale*

$$l_f \leq l_p \tag{7}$$

such that the regularized crack zone lies inside of the plastic zone as sketched in Fig. 1. The function $\widehat{\gamma}$ in (6) already appears in the approximation by Ambrosio and Tortorelli (1990) of the Mumford and Shah (1989) functional of image segmentation. The functional $\Gamma_l(d)$ converges to sharp-crack topology for vanishing fracture length scale $l_f \to 0$ as schematically visualized in Fig. 2, which depicts in addition a possible higher order approximation suggested by Borden et al. (2014). When assuming a given sharp crack surface topology by prescribing the Dirichlet condition $d=1$ on $\Gamma \subset \mathscr{B}_0$, the regularized crack phase field d in the full domain $\mathscr{B}_0$ is obtained by a *minimization principle of diffusive crack topology* with the limit

$$\lim_{l_f \to 0} \left\{ \inf_d \Gamma_l(d) \right\} = \Gamma(t), \tag{8}$$

see Miehe et al. (2010a) for more details. Fig. 3 depicts numerical solutions of this variational problem in two-dimensional setting, which demonstrate the influence of the fracture length scale l_f. Note that the limit for vanishing fracture length scale $l_f \to 0$ gives the sharp crack surface Γ. The crack phase field d is passive in the sense that an external driving is not allowed. Only time-independent ("passive") Dirichlet- and Neumann-conditions

$$d = 1 \ \text{ on } \ \Gamma \subset \mathscr{B}_0 \quad \text{and} \quad \nabla d \cdot \boldsymbol{n}_0 = 0 \ \text{ on } \ \partial \mathscr{B}_0 \tag{9}$$

are allowed, defining a sharp "initial crack" and "free" evolution of the crack phase field on the full boundary.

2.3. Global primary fields and constitutive state variables

The above introduced variables will characterize a multi-field setting of gradient plasticity at fracture based on three *global primary fields*

$$\mathfrak{U} := \{\boldsymbol{\varphi}, \alpha, d\}, \tag{10}$$

the finite deformation map $\boldsymbol{\varphi}$, the strain-hardening variable α and the crack phase field d. In addition, the plastic strain field $\boldsymbol{\varepsilon}^p$ serves as an additional *local primary field*. The subsequent constitutive approach to the phase field modeling of ductile fracture focuses on the set

$$\mathfrak{C} := \{\nabla\boldsymbol{\varphi}, \boldsymbol{\varepsilon}^p, \alpha, \nabla\alpha, d, \nabla d\}, \tag{11}$$

reflecting a combination of first-order gradient plasticity with a first-order gradient damage modeling. The state $\mathfrak{C}$ is considered as automatically objective, due to the dependence on the deformation gradient $\nabla\boldsymbol{\varphi}$ through the Lagrangian Hencky strain $\boldsymbol{\varepsilon}$ defined in (2). The subsequent theory of gradient plasticity at fracture uses these set of constitutive state variables.

3. Variational phase field approach to ductile fracture

This section outlines a theory for the coupling of gradient plasticity coupled with a phase field modeling of fracture that is fully variational in nature. It is based on the definition of constitutive work density and threshold functions, which define a *minimization principle* for the coupled evolution system.

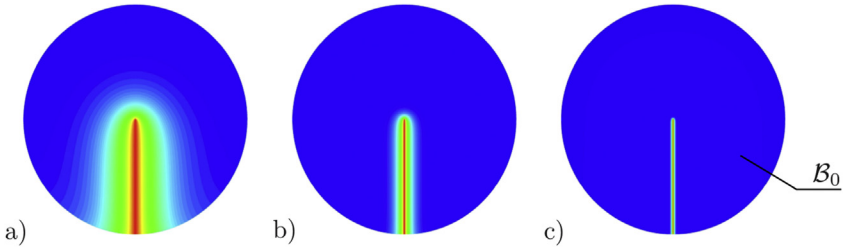

Fig. 3. Continuum approximation of crack discontinuities. Solutions of the variational problem (8) of diffusive crack topology for a circular specimen with a given sharp crack Γ, prescribed by the Dirichlet condition $d = 1$. Crack phase field $d \in [0, 1]$ for different length scales $l_f^a > l_f^b > l_f^c$. The sequence of plots visualizes the limit $\Gamma_l \to \Gamma$ of the regularized crack surface functional (8) towards the sharp crack surface.

3.1. Coupling gradient plasticity to gradient damage mechanics

Consider the stress power acting on a local material element that undergoes elastic–plastic deformation and damage $\mathscr{P} := \boldsymbol{\sigma} : \dot{\boldsymbol{\varepsilon}}$. It is the inner product of stress and rate of strain, the thermodynamic external variables acting on the material element. We use the Lagrangian logarithmic Hencky tensor $\boldsymbol{\varepsilon}$ defined in (2) and its dual stress tensor $\boldsymbol{\sigma}$. Let W denote the time-accumulated work per unit volume and $\mathscr{W}$ its accumulation in space

$$W := \int_0^T \mathscr{P} dt \quad \text{and} \quad \mathscr{W} := \int_{\mathscr{B}_0} W dV, \tag{12}$$

i.e. the total work needed to deform and crack the solid $\mathscr{B}_0$ within the process time $[0,T]$. We base the subsequent development of a phase field approach on a constitutive representation of this work

$$\mathscr{W} = \int_{\mathscr{B}_0} \left[\widehat{W}(\mathfrak{C}) + D_{vis} \right] dV. \tag{13}$$

It is governed by a *constitutive work density function* $\widehat{W}$ that describes the *rate-independent part* of the global work $\mathscr{W}$. The a priori dissipative *rate-dependent part* D_{vis} due to viscous resistance forces vanishes in the rate-independent limit. Equation (13) holds for particular boundary conditions of the "non-local" generalized internal variable fields α and d. These must be "passive" in the sense that an external driving of these fields is not allowed, which is consistent with (i) *constant Dirchlet data* and (ii) *zero Neumann data* of α and d on the surface $\partial\mathscr{B}_0$ of the solid, as defined in (4) and (9) above. The rate-independent part $\widehat{W}$ is assumed to depend on the array $\mathfrak{C}$ of constitutive state variables introduced in (11). We focus on the particular structure

$$\widehat{W}(\mathfrak{C}) = \widehat{g}(d)\widehat{w}_0^{ep}(\varepsilon^e, \alpha, \nabla\alpha) + (1 - \widehat{g}(d))w_c + 2\frac{w_c}{\zeta} l_f \widehat{\gamma}(d, \nabla d) \tag{14}$$

already suggested in Miehe et al. (2015), which provides a particular coupling of gradient plasticity with gradient damage mechanics. The function $\widehat{w}_0^{ep}$ splits up into elastic and plastic contributions according to

$$\widehat{w}_0^{ep}(\boldsymbol{\varepsilon}^e, \alpha, \nabla\alpha) = \widehat{w}_0^e(\boldsymbol{\varepsilon}^e) + \widehat{w}_0^p(\alpha, \nabla\alpha). \tag{15}$$

The derivatives of the potential density $\widehat{W}$ determine the rate-independent parts of stresses, the driving forces and the thresholds for the evolution of the plastic strains and the fracture phase field. It is based on four constitutive functions with a clear physical meaning:

F1. The *effective elastic work density function* $\widehat{w}_0^e$ models the stress response and the plastic driving force of the undamaged material.

F2. The *effective plastic work density function* $\widehat{w}_0^p$ models the local and strain gradient plastic hardening response of the undamaged material.

F3. The *degradation function* $\widehat{g}(d)$ describes the transition of the elastic–plastic work density $\widehat{w}_0^{ep}$ towards the constant crack threshold parameter w_c.

F4. The *crack surface density function* $\widehat{\gamma}(d, \nabla d)$ provides the geometric regularization of a sharp crack topology as already discussed above.

The work-density function $\widehat{W}$ models for $d \in [0, 1]$ with the first two terms a phase transition of the effective elastic–plastic work density $\widehat{w}_0^{ep}$ towards the constant threshold value w_c, and with the third term the accumulated fracture work density. Here, $w_c > 0$ is a *specific critical fracture energy* per unit volume, that enters the formulation as the key material parameter on the side of fracture mechanics. The second material parameter ζ *controls the post-critical range* after crack initialization by

scaling the work needed for the generation of the regularized crack surface. Fig. 4 gives a visual interpretation of the parameters w_c and ζ for a local homogeneous response, where $D^{pf}:=(1+1/\zeta)w_c$, defined in (26), is the maximum dissipated work density at fracture $d=1$. The constitutive representation for $\widehat{W}$ in (14) provides the basis for the coupling of a model of gradient plasticity (governed by $\widehat{w}_0^p$) with a gradient damage formulation (governed by $\widehat{\gamma}$), realized by the degradation function $\widehat{g}$.

3.2. Effective elastic-plastic work and degradation functions

3.2.1. Effective elastic work density

The effective elastic work density function $\widehat{w}_0^e$ in (15) models the stored elastic energy of the unbroken material, depending on the elastic strain measure $\boldsymbol{\varepsilon}^e$. For the subsequent model problems, the elastic work density is assumed to have the simple quadratic form

$$\widehat{w}_0^e(\boldsymbol{\varepsilon}^e) = \frac{\kappa}{2}\mathrm{tr}^2[\boldsymbol{\varepsilon}^e] + \mu\mathrm{tr}\Big[\mathrm{dev}(\boldsymbol{\varepsilon}^e)^2\Big], \tag{16}$$

characterizing an isotropic, linear stress response in the logarithmic strain space. Such an elastic stored energy has been considered by Anand (1979). See Miehe et al. (2014) for a more complex anisotropic setting. $\kappa>0$ and $\mu>0$ are the elastic bulk and the shear modulus, respectively. The function provides a structure identical to the geometrical linear theory of elasticity at small strains. Note that $\widehat{w}_0^e$ is *convex* with respect to $\boldsymbol{\varepsilon}^e$, however, due to the nonlinear relationship (1), *not poly-convex* with respect to $\boldsymbol{F}$. This restricts the model of elasto-plasticity under consideration to a range of small elastic strains $\|\varepsilon^e\|<\varepsilon$, however, accompanied by large plastic strain. This is a typical scenario applicable to metal plasticity.

3.2.2. Effective plastic work density

The effective plastic work density function $\widehat{w}_0^p$ in (15) models the dissipated plastic work of the unbroken material per unit volume, in terms of variables which describe the strain gradient hardening effect. For the modeling of length scale effects in isotropic gradient plasticity, we focus on the equivalent plastic strain α and its gradient. It is assumed to have the form

$$\widehat{w}_0^p(\alpha,\nabla\alpha) = \int_0^\alpha \widehat{y}(\tilde{\alpha})d\tilde{\alpha} + y_0\frac{l_p^2}{2}|\nabla\alpha|^2, \tag{17}$$

where $l_p\geq 0$ is a plastic length scale related to a strain-gradient hardening effect. $\widehat{y}(\alpha)$ is an isotropic local hardening function obtained form homogeneous experiments. We use in what follows the saturation-type function

$$\widehat{y}(\alpha) = y_o + (y_\infty - y_0)(1-\exp[-\eta\alpha]) + h\alpha \tag{18}$$

in terms of the four material parameters $y_0>0$, $y_\infty\geq y_0$, $\eta>0$ and $h\geq 0$, where the initial yield stress y_0 determines the threshold of the effective elastic response.

3.2.3. Degradation function

The degradation function $\widehat{g}(d)$ in (14) models the degradation of the elastic–plastic work density due to fracture. It interpolates between the unbroken response for $d=0$ and the fully broken state at $d=1$ by satisfying the constraints $\widehat{g}(0)=1$, $\widehat{g}(1)=0$, $\widehat{g}'(d)\leq 0$ and $\widehat{g}'(1)=0$. In particular, the last constraint ensures that the local driving force dual to d ensures an upper bound of the phase field $d\in[0,1]$. A function that satisfies this constraint is

$$\widehat{g}(d) = (1-d)^2. \tag{19}$$

The quadratic nature of this function is an important ingredient for the construction of a *linear equation* for the evolution of the phase field d. Note that the total work density $\widehat{W}$ introduced in (14) applies the same degradation function $\widehat{g}(d)$ on the effective elastic and plastic work densities $\widehat{w}_0^e$ and $\widehat{w}_0^p$, respectively. This is an important assumption with regard to the subsequent construction of a *gradient plasticity model related to the effective quantities* of the undamaged material, where the effective plastic work density $\widehat{w}_0^p$ serves as a ductile contribution to the crack driving force.[2]

[2] The functions $\widehat{g}$ defined in (19) appears in the Γ-convergent regularization by Ambrosio and Tortorelli (1990) of the Mumford-Shah functional in image segmentation, see Mumford and Shah (1989). Subsequently, it has been used by Bourdin et al. (2000) in the incremental approximation of their variational theory of brittle fracture Francfort and Marigo (1998), see also Comi (1999) for an early application in gradient damage mechanics. Note that the function (13) is *convex* with $\widehat{g}''>0$. This is in contrast to the non-convex function $\widehat{g}(d)=4(1-d)^3-3(1-d)^4$ used in the phase field model of Hakim and Karma (2009) in brittle fracture mechanics.

3.3. Stored energy, dissipation and thermodynamic consistency

3.3.1. Energetic-dissipative split

In order to quantify both the energy stored in the material and the dissipation, a further assumption is needed that postulates a split of the work density function $\widehat{W}$ into energetic and dissipative parts. To this end, (14) is decomposed

$$\widehat{W}(\mathfrak{C}) = \widehat{\psi}^{e}(\varepsilon^{e}, d) + \widehat{D}^{pf}(\alpha, \nabla\alpha, d, \nabla d) \tag{20}$$

into a *stored energy density* $\widehat{\psi}^{e}$ and the *accumulated dissipative part* $\widehat{D}^{pf}$ due to plasticity and fracture. This split assumes that the macroscopic elastic strain energy is the only part of the total work density that is stored in the material. The constitutive expression for this part obtained from (14) is

$$\widehat{\psi}^{e}(\boldsymbol{\varepsilon}^{e}, d) = \widehat{g}(d)\widehat{w}_0^{e}(\boldsymbol{\varepsilon}^{e}) \tag{21}$$

governed by the degradation function $\widehat{g}$ and the elastic strain energy function $\widehat{w}_0^{e}$ of the unbroken material.[3] Consequently, the remaining part of the work density function (14)

$$\widehat{D}^{pf}(\alpha, \nabla\alpha, d, \nabla d) = \widehat{g}(d)\widehat{w}_0^{p}(\alpha, \nabla\alpha) + (1 - \widehat{g}(d))w_c + 2\frac{w_c}{\zeta}l_f\widehat{\gamma}(d, \nabla d) \tag{22}$$

models the accumulated dissipation in terms of the plastic work density function $\widehat{w}_0^{p}$ of the unbroken material and the crack surface density function $\widehat{\gamma}$.

3.3.2. Plasticity-fracture split

Note that $\widehat{D}^{pf}$ provides a constitutive expression for the accumulated dissipation due to plasticity *and* fracture. It does not allow to separate both contributions. In order to investigate this, define the dissipation *locally* as the difference of the external stress power and the evolution of the energy storage, by the standard Clausius-Planck inequality

$$\mathscr{D}^{pf} := \boldsymbol{\sigma} : \dot{\boldsymbol{\varepsilon}} - \frac{d}{dt}\widehat{\psi}^{e} \geq 0. \tag{23}$$

Applying a standard argument, a reduced expression for this dissipation splits up into plastic and fracture parts

$$\mathscr{D}^{pf} := \mathscr{D}^{p} + \mathscr{D}^{f} \geq 0 \quad \text{with} \quad \mathscr{D}^{p} := \boldsymbol{f}^{p} : \dot{\boldsymbol{\varepsilon}}^{\boldsymbol{p}} \geq 0 \quad \text{and} \quad \mathscr{D}^{f} := f^{f}\dot{d} \geq 0 \tag{24}$$

in terms of the energetic plastic and fracture *driving forces*

$$\boldsymbol{f}^{p} := -\partial_{\boldsymbol{\varepsilon}^{p}}\widehat{\psi}^{e} = -\widehat{g}\partial_{\boldsymbol{\varepsilon}^{p}}\widehat{w}_0^{e} \quad \text{and} \quad f^{f} := -\partial_{d}\widehat{\psi}^{e} = -\partial_{d}\widehat{g}\,\widehat{w}_0^{e} \tag{25}$$

obtained from the energy storage function $\widehat{\psi}^{e}$ in (21). When introducing the time- and space-accumulated dissipative work

$$D^{pf} := \int_0^T \mathscr{D}^{pf}\,dt \quad \text{and} \quad \boldsymbol{D}^{pf} := \int_{\mathscr{B}_0} D^{pf}\,dV, \tag{26}$$

in analogy to (12), insertion of (24) allows a *separate identification* of the contributions due to plasticity and fracture. In particular, we have

$$D^{pf} := D^{p} + D^{f} \tag{27}$$

with the definitions

[3] This assumption does not specify the stored energy due to cold (plastic) work, that is difficult to quantify by caloric experiments. In that sense, (21) provides a convenient mathematical definition suitable for *pure mechanical* analyses.

$$D^p := \int_0^{\boldsymbol{\varepsilon}^p} \boldsymbol{f}^p : d\tilde{\boldsymbol{\varepsilon}}^p \quad \text{and} \quad D^f := \int_0^{d} f^f \, d\tilde{d}. \tag{28}$$

These expressions can numerically be evaluated and provide for a rate-independent model with $D_{vis} = 0$ in (13) under homogeneous conditions with $\nabla\alpha = \nabla d = 0$ the closed form $\widehat{D}^{pf}$ in (22). The split (27) is visualized in Fig. 4 below for a one-dimensional model problem of non-hardening ideal plasticity.

3.4. Driving, resistance and thresholds for plasticity and fracture

The evolution of the plastic strains and fracture phase field is constructed in a normal-dissipative format related to threshold functions. These functions are formulated in terms of energetic driving forces and dissipative resistance forces, related to the split (20) of the work density function $\widehat{W}$ into the energetic and dissipative parts $\widehat{\psi}^e$ and $\widehat{D}^{pf}$.

3.4.1. Threshold for plasticity

The energetic driving force dual to the plastic strain $\boldsymbol{\varepsilon}^p$ and the rate independent part of the dissipative resistance dual to the hardening variable α are defined by

$$\boldsymbol{f}^p := -\partial_{\boldsymbol{\varepsilon}^p} \widehat{\psi}^e \quad \text{and} \quad r^p := \delta_\alpha \widehat{D}^{pf}. \tag{29}$$

Here, $\delta_\alpha \widehat{D}^{pf} := \partial_\alpha \widehat{D}^{pf} - \text{Div}[\partial_{\nabla\alpha} \widehat{D}^{pf}]$ denotes the variational derivative of $\widehat{D}^{pf}$ by α, reflecting characteristics of the gradient-extended plasticity model under consideration. Clearly, for the kinematic assumption (1), the energetic driving force $\boldsymbol{f}^p$ is the stress tensor $\boldsymbol{\sigma}$ dual to the Hencky strain in the logarithmic strain space. An *elastic domain* associated with the plastic deformation in the space of the plastic driving force is defined by

$$\mathbb{E}_{plas} := \left\{ (\boldsymbol{f}^p, r^p) \,\middle|\, \widehat{\phi}^p(\boldsymbol{f}^p, r^p) \le 0 \right\} \tag{30}$$

in terms of the *plastic yield function* $\widehat{\phi}^p$. We focus on the function

$$\widehat{\phi}^p(\boldsymbol{f}^p, r^p) = \|\text{dev}[\boldsymbol{f}^p]\| - \sqrt{\frac{2}{3}} r^p \tag{31}$$

of the von Mises type in the logarithmic stress space.[4]

3.4.2. Threshold for fracture

The energetic driving force and the rate-independent part of the dissipative resistance dual to the fracture phase field d are defined by

$$f^f := -\partial_d \widehat{\psi}^e \quad \text{and} \quad r^f := \delta_d \widehat{D}^{pf}. \tag{35}$$

[4] Gradient Plasticity in the Effective Stress Space. When using the constitutive structure for $\widehat{W}$ in (14), note that the above yield function can be recast into the form

$$\widehat{\phi}^p(\boldsymbol{f}^p, r^p) = \widehat{g}(d)\, \widehat{\phi}^p_0(\boldsymbol{f}^p_0, r^p_0) \quad \text{with} \quad \widehat{\phi}^p_0 = \|\text{dev}[\boldsymbol{f}^p_0]\| - \sqrt{\frac{2}{3}} r^p_0 \tag{32}$$

with the degradation function $\widehat{g}(d)$ defined in (19) and the *effective plastic yield function* formulated in terms of the *effective stress-like variables*

$$\boldsymbol{f}^p_0 := \frac{1}{\widehat{g}(d)} \boldsymbol{f}^p = -\partial_{\boldsymbol{\varepsilon}^p} \widehat{w}^e_0 \quad \text{and} \quad r^p_0 := \frac{1}{\widehat{g}(d)} r^p = \delta_\alpha \widehat{w}^p_0. \tag{33}$$

This constitutive structure characterizes a formulation of gradient plasticity related to the effective state variables of the undamaged material. Hence, $\mathbb{E}_{plas}$ in (30) can be interpreted to bound the domain

$$\mathbb{E}^0_{plas} := \left\{ (\boldsymbol{f}^p_0, r^p_0) \,\middle|\, \widehat{\phi}^p_0(\boldsymbol{f}^p_0, r^p_0) \le 0 \right\} \tag{34}$$

in the effective stress space. Note that the von Mises condition (31), that neglects volumetric plastic flow, is used as a conceptual example of the variational theory presented here.

The variational derivative $\delta_d \widehat{D}^{pf} := \partial_d \widehat{D}^{pf} - \mathrm{Div}[\partial_{\nabla d} \widehat{D}^{pf}]$ characterizes the phase field model of fracture as a gradient-extended damage formulation. A *crack resistance domain* associated with the crack propagation in the space of the crack driving force is defined by

$$\mathbb{E}_{frac} := \left\{ \left(f^f - r^f \right) \Big| \widehat{\phi}^f \left(f^f - r^f \right) \leq 0 \right\} \tag{36}$$

in terms of the *crack threshold function* $\widehat{\phi}^f$. We focus on the constitutive representation

$$\widehat{\phi}^f \left(f^f - r^f \right) = f^f - r^f . \tag{37}$$

where the energetic driving force f^f is bounded by the crack resistance r^f.

3.5. Evolution equations for the generalized internal variables

3.5.1. Introduction of a dissipation potential function

With the above introduced threshold and resistance functions at hand, a dissipation potential function can be constructed based on the standard concept of maximum dissipation. For a rate-independent evolution of the inelastic state, this defines the potential function

$$\widehat{V}(\dot{\mathfrak{C}}) = \sup_{(\boldsymbol{f}^p, r^p) \in \mathbb{E}_{plas}} \sup_{(f^f - r^f) \in \mathbb{E}_{frac}} \left[\boldsymbol{f}^p : \dot{\boldsymbol{\varepsilon}}^p - r^p \dot{\alpha} + \left(f^f - r^f \right) \dot{d} \right] \tag{38}$$

related to the two elastic domains $\mathbb{E}_{plas}$ and $\mathbb{E}_{frac}$ defined in (30) and (36), respectively. Note that this normal-dissipative evolution response is governed by only two scalar functions.

F5. The *plastic yield function* $\widehat{\phi}^p(\boldsymbol{f}^p, r^p)$ that determines the elastic domain in terms of the plastic driving force.

F6. The *fracture threshold function* $\widehat{\phi}^f(f^f - r^f)$ that determines the initiation of fracture in terms of the fracture driving force.

These two functions, defined for the model problem under consideration in (31) and (37), supplement the four constitutive functions $\widehat{w}_0^e$, $\widehat{w}_0^p$, $\widehat{g}$ and $\widehat{\gamma}$ in the total work density function (12) and complete the proposed phase field model of fracture.

3.5.2. Rate-independent evolution

For the rate-independent evolution, the constrained optimization problem (38) is solved via an extended Lagrange functional

$$\widehat{V}(\dot{\mathfrak{C}}) = \sup_{\boldsymbol{f}^p, r^p, f^f - r^p} \sup_{\lambda^p, \lambda^f} \Big[\boldsymbol{f}^p : \dot{\boldsymbol{\varepsilon}}^p - r^p \dot{\alpha} + \left(f^f - r^r \right) \dot{d} - \lambda^p \widehat{\phi}^p(\boldsymbol{f}^p, r^p) - \lambda^f \widehat{\phi}^f \left(f^f - r^r \right) \Big], \tag{39}$$

where the Lagrange parameters λ^p and λ^f control the non-smooth evolution of the plasticity and the fracture, respectively. The necessary conditions of the local optimization problem (39) determine the *plastic flow rules*

$$\dot{\boldsymbol{\varepsilon}}^p = \lambda^p \partial_{\boldsymbol{f}^p} \widehat{\phi}^p \quad \text{and} \quad \dot{\alpha} = -\lambda^p \partial_{r^p} \widehat{\phi}^p \tag{40}$$

and the normal-dissipative *evolution equation for the crack phase field*

$$\dot{d} = \lambda^f \partial_{f^f - r^r} \widehat{\phi}^f . \tag{41}$$

along with the two loading-unloading conditions

$$\lambda^p \geq 0, \widehat{\phi}^p \leq 0, \lambda^p \widehat{\phi}^p = 0 \quad \text{and} \quad \lambda^f \geq 0, \widehat{\phi}^f \leq 0, \lambda^f \widehat{\phi}^f = 0. \tag{42}$$

of the plastic and fracture response, respectively.

3.5.3. Viscous regularized evolution

In this work, we consider *viscous regularizations* for both dissipation mechanisms. This allows the definition of a dissipation potential function in a non-constrained manner

$$\widehat{V}(\dot{\mathfrak{C}}) = \sup_{\boldsymbol{f}^p, r^p, f^f - r^f} \Big[\boldsymbol{f}^p : \dot{\boldsymbol{\varepsilon}}^p - r^p \dot{\alpha} + \Big(f^f - r^f \Big) \dot{d} - \widehat{V}^* \Big(\boldsymbol{f}^p, r^p, f^f - r^f \Big) \Big], \tag{43}$$

in terms of the *dual dissipation potential function*

$$\widehat{V}^* \Big(\boldsymbol{f}^p, r^p, f^f - r^f \Big) = \frac{3}{4\eta_p} \langle \widehat{\phi}^p (\boldsymbol{f}^p, r^p) \rangle^2 + \frac{1}{2\eta_f} \langle \widehat{\phi}^f \Big(f^f - r^f \Big) \rangle^2 \tag{44}$$

where $\langle x \rangle := (x + |x|)/2$ is the Macaulay bracket. η_p and η_f are additional material parameters which characterize viscosity of the plastic deformation and the crack propagation. Note that the dual dissipation potential $\widehat{V}^*$ in (43) can mathematically be interpreted as a quadratic penalty term, that enforces approximately the threshold conditions (30) and (36). The necessary conditions of the local optimization problem (43) yield the *plastic flow rules* (40) and the *evolution equation for the crack phase field* (41), where the loading-unloading conditions (42) are replaced by the viscous constitutive functions

$$\lambda^p := \frac{3}{2\eta_p} \langle \widehat{\phi}^p \rangle \geq 0 \quad \text{and} \quad \lambda^f := \frac{1}{\eta_f} \langle \widehat{\phi}^f \rangle \geq 0. \tag{45}$$

Furthermore, note that the positiveness of the parameters λ^p and λ^f imply via (40) and (41) a *monotonic growth*

$$\dot{\alpha} \geq 0 \quad \text{and} \quad \dot{d} \geq 0 \tag{46}$$

of the equivalent plastic strain and the fracture phase field.

3.6. Proof of thermodynamic consistency and its consequences

The above evolution equations (40) and (41) satisfy the thermodynamic constraints (24). In particular, we have

$$\mathscr{D}^p = \| \mathrm{dev}[\boldsymbol{f}^p] \| \lambda^p \geq 0 \quad \text{and} \quad \mathscr{D}^f = f^f \lambda^f \geq 0. \tag{47}$$

This is obvious due to the a priori positive parameters λ^p and λ^f and the positive driving terms, caused by the *convexity of the threshold functions* $\widehat{\phi}^p$ and $\widehat{\phi}^f$ in (31) and (37), respectively. For the case of both plastic as well as fracture loading with $\widehat{\phi}^p \geq 0$ and $\widehat{\phi}^f \geq 0$, the driving forces can be expressed in terms of the rate-independent and rate-dependent resistances

$$\| \mathrm{dev}[\boldsymbol{f}^p] \| = \sqrt{\frac{2}{3}} \Big(r^p + \eta_p \dot{\alpha} \Big) \quad \text{and} \quad f^f = r^f + \eta_f \dot{d}, \tag{48}$$

yielding the representation of the dissipation

$$\mathscr{D}^p = r^p \dot{\alpha} + \eta_p \dot{\alpha}^2 \geq 0 \quad \text{and} \quad \mathscr{D}^f = r^f \dot{d} + \eta_f \dot{d}^2 \geq 0. \tag{49}$$

Hence, the total dissipation splits into rate-independent and rate-dependent parts

$$\mathscr{D} := \mathscr{D}^{pf} + \mathscr{D}_{vis} \geq 0 \quad \text{with} \quad \mathscr{D}^{pf} = r^p \dot{\alpha} + r^f \dot{d} \quad \text{and} \quad \mathscr{D}_{vis} := \eta_p \dot{\alpha}^2 + \eta_f \dot{d}^2. \tag{50}$$

The viscous part is positive for positive material parameters $\eta_p > 0$ and $\eta_f > 0$. Using the definitions of r^p and r^f in (29) and (35) in terms of variational derivatives of the function $\widehat{D}^{pf}$, the integration over the volume of the solid gives

$$\int_{\mathscr{B}_0} \mathscr{D} dV = \int_{\mathscr{B}_0} \Big[\frac{d}{dt} \widehat{D}^{pf} + \mathscr{D}_{vis} \Big] dV - \int_{\partial \mathscr{B}_0} \Big[\partial_{\nabla \alpha} \widehat{D}^{pf} \cdot \boldsymbol{n}_0 \dot{\alpha} + \partial_{\nabla d} \widehat{D}^{pf} \cdot \boldsymbol{n}_0 \dot{d} \Big] dA \geq 0. \tag{51}$$

Here, the surface term vanishes as a consequence of the restriction to “passive” boundary conditions, representing (i) *constant Dirchlet data* and (ii) *zero Neumann data* of α and d on the surface $\partial \mathscr{B}_0$ of the solid, see (61) below for further details. When integrating over the process time $[0,T]$, we end up with the representation of the space-time-accumulated *total dissipative work* needed for the generation of plastic deformation and fracture

$$\boldsymbol{D} := \int_{\mathscr{B}_0} \Big[\widehat{D}^{pf}(\alpha, \nabla\alpha, d, \nabla d) + D_{vis} \Big] dV \geq 0 \tag{52}$$

with the definition

$$D_{vis} := \int_0^T \mathscr{D}_{vis} dt \geq 0. \tag{53}$$

This identifies the dissipative part of the work density function $\widehat{W}$ introduced in (14) with decomposition (20) as the time-space-accumulated dissipative work done to the solid.

3.7. Role of material parameters for brittle and ductile fracture

The onset of fracture and plasticity is governed by the critical work density w_c in (14) and the initial yield stress y_0 in (18), respectively. The relationship of these two key material parameters on dissipative side to the elastic moduli κ and μ in (16) makes the difference between brittle or ductile fracture.

3.7.1. Brittle fracture

Brittle fracture is initiated by a crack evolution that is followed by a plastic deformation. In other words, the elastic initial deformation reaches a critical state that triggers a brittle crack before plasticity starts. This scenario comes for the condition at the onset of fracture

$$\widehat{\phi}^f\left(f^f, 2w_c\right) = 0 \quad \text{and} \quad \widehat{\phi}^p(\boldsymbol{f}^p, y_0) < 0 \tag{54}$$

of the threshold functions introduced above. The combination of these two conditions gives a constraint on the material parameters

$$\text{Brittle E} - \text{F} - \text{P Response}: \quad w_c - \frac{\kappa}{2}\text{tr}^2[\boldsymbol{\varepsilon}] < \frac{1}{3}\frac{y_0^2}{2\mu} \tag{55}$$

that depends on the volumetric strain state. It states that a critical deviatoric energy for fracture is less than the deviatoric energy that triggers plasticity. The onsets of fracture and subsequent plasticity are then defined by the criteria

$$\text{Onset F}: \frac{\kappa}{2}\text{tr}^2[\boldsymbol{\varepsilon}] + \mu\|\text{dev}[\boldsymbol{\varepsilon}]\|^2 = w_c \quad \text{and} \quad \text{Onset P}: \mu\|\text{dev}[\boldsymbol{\varepsilon}]\|^2 = \frac{1}{3}\frac{y_0^2}{2\mu}. \tag{56}$$

The fracture starts when the elastic energy reaches the critical value w_c. A further increase of strain $\boldsymbol{\varepsilon}$ results in an evolving fracture phase field d. The subsequent onset of plasticity then occurs if the effective deviatoric strain energy reaches the critical energy for plastic yielding.

3.7.2. Ductile fracture

Ductile fracture is characterized by a plastic yielding before fracture. This scenario is associated with the condition at the onset of plasticity

$$\widehat{\phi}^p(\boldsymbol{f}^p, y_0) = 0 \quad \text{and} \quad \widehat{\phi}^f\left(\boldsymbol{f}^f, 2w_c\right) < 0 \tag{57}$$

of the two threshold functions. The combination of these two conditions gives the constraint on the material parameters

$$\text{Ductile E} - \text{P} - \text{F Response}: \quad w_c - \frac{\kappa}{2}\text{tr}^2[\boldsymbol{\varepsilon}] > \frac{1}{3}\frac{y_0^2}{2\mu}. \tag{58}$$

Here, the critical deviatoric energy that triggers fracture exceeds the deviatoric energy at the onset of plasticity. The onsets of plasticity and subsequent fracture are then defined by

$$\text{Onset P}: \mu\big\|\text{dev}[\boldsymbol{\varepsilon}]\big\|^2 = \frac{1}{3}\frac{y_0^2}{2\mu} \quad \text{and} \quad \text{Onset F}: \frac{\kappa}{2}\text{tr}^2[\boldsymbol{\varepsilon}] + \frac{1}{3}\frac{\widehat{y}(\alpha)^2}{2\mu} + \int_0^\alpha \widehat{y}(\tilde{\alpha}) d\tilde{\alpha} = w_c. \tag{59}$$

of a homogeneous plastic state with $\nabla\alpha = 0$. Plasticity starts if the deviatoric elastic energy reaches the critical value for yielding. A further increase of strain $\boldsymbol{\varepsilon}$ results in evolving equivalent plastic strain α. The subsequent onset of fracture then occurs if the sum of *effective* deviatoric strain energy and *effective* plastic work density reaches the critical value for ductile fracture.

Note that for a homogeneous deformation process that is approximately isochoric, i.e. $\mathrm{tr}[\boldsymbol{\varepsilon}] \approx 0$, the critical work density w_c for the onset of fracture can be estimated in terms of a *critical value* α_c *of the equivalent plastic strain*. $(59)_2$ then induces the estimate

$$w_c \approx \frac{1}{3}\frac{\widehat{y}(\alpha_c)^2}{2\mu} + \int_0^{\alpha_c} \widehat{y}(\tilde{\alpha})\, d\tilde{\alpha} \tag{60}$$

of w_c in terms of a given α_c based on a given local hardening function $\widehat{y}(\alpha)$ such as (18). The choice (19) of the degradation function $\widehat{g}$ allows a further interpretation of the material parameters w_c and ζ introduced in (14). A bound of the effective elastic–plastic work function $\widehat{w}_0^{ep}$ due to plasticity and fracture is per definition the work density function $\widehat{W}$ evaluated at $d = 1$. Hence,

$$\widehat{D}^{pf}(\alpha, 0, 1, 0) = \left(1 + \frac{1}{\zeta}\right) w_c \tag{61}$$

is the maximum value of the dissipated work density for a *homogeneous rate-independent process*, see Fig. 4 below. For a given fracture threshold parameter w_c, the parameter $\zeta \leq 1$ scales the dissipative work, providing for $\zeta < 1$ an increase of the dissipation due to fracture.

4. Minimization principle for the evolution problem

4.1. Minimization principle for the multi-field evolution problem

With the above introduced functions at hand, the boundary value problem is fully governed by a rate-type minimization principle for the quasi-static case, where inertia effects are neglected. In line with recent treatments on variational principles of gradient-extended materials outlined in Miehe (2011), consider the constitutive rate potential density

$$\pi(\dot{\mathfrak{C}}) = \frac{d}{dt}\widehat{W}(\mathfrak{C}) + \widehat{V}(\dot{\mathfrak{C}}) \tag{62}$$

in terms of the basic constitutive functions $\widehat{W}$ and $\widehat{V}$ defined in (14) and (43), respectively. With this potential density at hand, the evolution of the boundary-problem of gradient plasticity coupled with gradient damage mechanics is governed by the *global rate potential*

$$\Pi\left(\dot{\boldsymbol{\varphi}}, \dot{\alpha}, \dot{d}, \dot{\boldsymbol{\varepsilon}}^p\right) = \int_{\mathscr{B}_0} \pi(\dot{\mathfrak{C}})\, dV - P_{ext}(\dot{\boldsymbol{\varphi}}) \tag{63}$$

where $P_{ext}(\dot{\boldsymbol{\varphi}}) := \int_{\mathscr{B}_0} \overline{\boldsymbol{\gamma}}_0 \cdot \dot{\boldsymbol{\varphi}}\, dV + \int_{\partial\mathscr{B}_0} \overline{\boldsymbol{t}}_0 \cdot \dot{\boldsymbol{\varphi}}\, da$ is an external load functional. $\overline{\boldsymbol{\gamma}}_0$ is a given body force per unit volume of the reference configuration, $\overline{\boldsymbol{t}}_0$ a given traction field on the surface of the reference configuration. The evolution of all primary fields introduced in Section 2 at a given state is determined by the *minimization principle*

$$\left\{\dot{\boldsymbol{\varphi}}, \dot{\alpha}, \dot{d}, \dot{\boldsymbol{\varepsilon}}^p\right\} = \mathrm{Arg}\left\{\inf_{\dot{\boldsymbol{\varphi}}, \dot{\alpha}, \dot{d}, \dot{\boldsymbol{\varepsilon}}^p} \Pi\left(\dot{\boldsymbol{\varphi}}, \dot{\alpha}, \dot{d}, \dot{\boldsymbol{\varepsilon}}^p\right)\right\}. \tag{64}$$

Here, the evolutions $\{\dot{\boldsymbol{\varphi}}, \dot{\alpha}, \dot{d}\}$ of the global fields are constrained by Dirichlet-type boundary conditions defined in (1), (4) and (9) above. Note that the minimization structure of this variational principle is governed by the *convexity of the dissipation potential function* $\widehat{V}$ in (43), which states the thermodynamical consistency with the second axiom of thermodynamics. The combination of the global minimization principle (64) with the local maximum problem (43) for the definition of the dissipation potential $\widehat{V}$ provides a *mixed variational principle*, that defines all equations of the problem of gradient plasticity at fracture. When introducing the *mixed potential density*

$$\pi^* = \frac{d}{dt}\widehat{W} + \boldsymbol{f}^p : \dot{\boldsymbol{\varepsilon}}^p - r^p\dot{\alpha} + \left(f^f - r^f\right)\dot{d} - \frac{3}{4\eta_p}\langle\widehat{\phi}^p\rangle^2 - \frac{1}{2\eta_f}\langle\widehat{\phi}^f\rangle^2, \tag{65}$$

the Euler equations of the variational principle (64) appear in the form

$$
\begin{aligned}
&1.\ \textit{Stress equilibrium} && \delta_{\widehat{\varphi}}\pi^* \equiv -\operatorname{Div}\Big[\partial_{\nabla\varphi}\widehat{W}\Big] = \overline{\gamma}_0 \\
&2.\ \textit{Hardening force} && \delta_{\widehat{\alpha}}\pi^* \equiv \partial_{\alpha}\widehat{W} - \operatorname{Div}\Big[\partial_{\nabla\alpha}\widehat{W}\Big] - r^p = 0 \\
&3.\ \textit{Fracture force} && \delta_{\widehat{d}}\pi^* \equiv \partial_{d}\widehat{W} - \operatorname{Div}\Big[\partial_{\nabla d}\widehat{W}\Big] + \Big(f^f - r^f\Big) = 0 \\
&4.\ \textit{Plastic force} && \partial_{\dot{\varepsilon}^p}\pi^* \equiv \partial_{\varepsilon^p}\widehat{W} + f^p = 0 \\
&5.\ \textit{Plastic strains} && \partial_{f^p}\pi^* \equiv \dot{\varepsilon}^p - \lambda^p\partial_{f^p}\widehat{\phi}^p = 0 \\
&6.\ \textit{Equivalent strain} && \partial_{r^p}\pi^* \equiv -\dot{\alpha} - \lambda^p\partial_{r^p}\widehat{\phi}^p = 0 \\
&7.\ \textit{Fracture phase field} && \partial_{(f^f - r^f)}\pi^* \equiv \dot{d} - \lambda^f\partial_{(f^f - r^f)}\widehat{\phi}^f = 0
\end{aligned}
\tag{66}
$$

along with Neumann-type boundary conditions of the form defined in (1), (4) and (9) above. The loading parameters λ^p and λ^f are defined in (45). Note that above Euler equations are exclusively related to variational derivatives of the potential density π^* defined in (65). More details of the Euler equations associated with the variational principle (64) are outlined in Section 4.3 below.

4.2. Numerical implementation of the minimization problem

4.2.1. Incremental potential density

We consider a finite time increment $[t_n, t_{n+1}]$, where $\tau_{n+1} := t_{n+1} - t_n > 0$ denotes the step length. All fields at time t_n are assumed to be *known*. The goal then is to determine the fields at time t_{n+1} based on variational principles valid for the time increment under consideration. Subsequently, all variables without subscript are evaluated at time t_{n+1}. Next, define the *mixed incremental potential density* per unit volume by an algorithmic approximation

$$
\pi^{*\tau}(\mathfrak{C}^*) = Algo\left\{ \int_{t_n}^{t_{n+1}} \pi^* dt \right\} \tag{67}
$$

in terms of the continuous rate-type potential π^* introduced in (65). Using a fully implicit Euler scheme gives

$$
\pi^{*\tau} = \widehat{W} + \boldsymbol{f}^p : (\boldsymbol{\varepsilon}^p - \boldsymbol{\varepsilon}^p_n) - r^p \cdot (\alpha - \alpha_n) + \Big(f^f - r^f\Big)(d - d_n) - \frac{3\tau}{4\eta_p}\langle\widehat{\phi}^p\rangle^2 - \frac{\tau}{2\eta_f}\langle\widehat{\phi}^f\rangle^2. \tag{68}
$$

The set $\mathfrak{C}^*$ of current state variables can be split up into *local part* $\mathfrak{C}^*_l$ associated with variables related to local ODEs and a *global part* $\mathfrak{C}^*_g$ associated with variables related to global PDEs

$$
\mathfrak{C}^*_l := \{\boldsymbol{\varepsilon}^p, \boldsymbol{f}^p\} \quad \text{and} \quad \mathfrak{C}^*_g := \Big\{\nabla\boldsymbol{\varphi}, \alpha, \nabla\alpha, d, \nabla d, r^p, f^f - r^f\Big\}. \tag{69}
$$

According to this split, the solution procedure for the update of the state variables is split up in a local and a global part.

4.2.2. Condensation of local variables

The first part of the incremental solution procedure consist of condensation of the incremental potential density $\pi^{*\tau}$ by the set of local variables assembled in $\mathfrak{C}^*_l$ by defining *condensed incremental work density*

$$
(L): \pi^{*\tau}_{red}\Big(\mathfrak{C}^*_g\Big) = \inf_{\boldsymbol{\varepsilon}^p} \sup_{\boldsymbol{f}^p} \pi^{*\tau}(\mathfrak{C}^*). \tag{70}
$$

The necessary conditions of this local problem are

$$
\partial_{\mathfrak{C}^*_l}\pi^{*\tau}(\mathfrak{C}^*) = \begin{bmatrix} \partial_{\boldsymbol{\varepsilon}^p}\widehat{W} + \boldsymbol{f}^p \\ \boldsymbol{\varepsilon}^p - \boldsymbol{\varepsilon}^p_n - \tau\lambda^p\partial_{\boldsymbol{f}^p}\widehat{\phi}^p \end{bmatrix} = 0, \tag{71}
$$

defining the plastic driving force $\boldsymbol{f}^p$ and the update of the plastic strains $\boldsymbol{\varepsilon}^p$.

4.2.3. Reduced global problem

With the condensed incremental work potential $\pi^{*\tau}_{red}$ defined in (70) at hand, define the reduced potential function

$$\Pi^{*\tau}_{red}\Big(\boldsymbol{\varphi},\alpha,d,r^p,f^f-r^f\Big)=\int\limits_{\mathscr{B}_0}\pi^{*\tau}_{red}\Big(\mathfrak{C}^*_g\Big)dV \tag{72}$$

for pure Dirichlet problems with $P_{ext}=0$ in (63). The second part of the incremental solution procedure consists of the solution of the mixed saddle point principle

$$(G):\Big\{\boldsymbol{\varphi},\alpha,d,r^p,f^f-r^f\Big\}=\text{Arg}\Big\{\inf_{\boldsymbol{\varphi},\alpha,d}\sup_{r^p,f^f-r^f}\Pi^{*\tau}_{red}\Big(\boldsymbol{\varphi},\alpha,d,r^p,f^f-r^f\Big)\Big\} \tag{73}$$

that determines the global fields and the associated driving forces. A straightforward finite element discretization of this problem based on interpolations

$$\mathfrak{C}^*_g(\boldsymbol{X},t)=\boldsymbol{B}^*(\boldsymbol{X})\boldsymbol{d}^*(t)\quad\text{with}\quad\boldsymbol{d}^*:=\Big\{\boldsymbol{\varphi},\alpha,d,r^p,f^f-r^f\Big\}_{I=1}^{N_{node}} \tag{74}$$

results in the necessary condition of the FE-discretized mixed variational principle (73), yielding the nonlinear algebraic system

$$\partial_{\boldsymbol{d}^*}\Pi^{*\tau h}_{red}=\int\limits_{\mathscr{B}_0}\boldsymbol{B}^{*T}\mathscr{S}^*dV=0. \tag{75}$$

Here, $\mathscr{S}^*$ is a generalized stress array dual to the global part $\mathfrak{C}^*_g$ of the state variables, defined by

$$\mathscr{S}^*:=\partial_{\mathfrak{C}^*_g}\pi^{*\tau}_{red}(\boldsymbol{B}^*\boldsymbol{d}^*)=\begin{bmatrix}\partial_{\nabla\boldsymbol{\varphi}}\widehat{W}\\ \partial_{\alpha}\widehat{W}-r^p\\ \partial_{\nabla\alpha}\widehat{W}\\ \partial_{d}\widehat{W}+\Big(f^f-r^f\Big)\\ \partial_{\nabla d}\widehat{W}\\ -\alpha+\alpha_n-\tau\lambda^p\partial_{r^p}\widehat{\phi}^p\\ d-d_n-\tau\lambda^f\partial_{(f^f-r^f)}\widehat{\phi}^f\end{bmatrix}, \tag{76}$$

where the constitutive parameters λ^p and λ^f are defined in (45). A difficulty of the numerical solution of the mixed variational principle (73) is the appropriate interpolation of the dual-primal problem that includes the driving forces r^p and f^f-r^p associated with the gradient plastic and the gradient damage effects. For the phase field model of brittle fracture, such an implementation is outlined in Miehe et al. (2010a). For gradient plasticity, the recent sequence of works Miehe et al. (2013, 2015) discussed details of the mixed finite element formulations.

4.3. The three governing PDEs of the multi-field problem

4.3.1. The stress equilibrium equation

The first Euler equation $(66)_1$ of the variational principle (64) is the quasi-static form of the balance of momentum, which follows by taking the variation of the potential Π in (63) with respect to $\boldsymbol{\varphi}$, yielding

$$\text{Div}\Big[(1-d)^2\boldsymbol{\sigma}_0:\mathscr{P}_{log}\Big]+\overline{\boldsymbol{\gamma}}_0=\boldsymbol{0}. \tag{77}$$

Here, the first Piola nominal stress $\boldsymbol{P}$ is obtained from the potential $\widehat{W}$ in (14) by

$$\boldsymbol{P}:=\partial_{\boldsymbol{F}}\widehat{W}=\boldsymbol{\sigma}:\mathscr{P}_{log}\quad\text{with}\quad\mathscr{P}_{log}:=\partial_{\boldsymbol{F}}\boldsymbol{\varepsilon}. \tag{78}$$

The *projection tensor* $\mathscr{P}_{log}$ projects the nominal Lagrangian Hencky tensor $\boldsymbol{\sigma}$ from the logarithmic strain space to the first Piola stress. An explicit form of this tensor based on a spectral representation is outlined in Miehe et al. (2002). The nominal Hencky tensor is related by

$$\boldsymbol{\sigma}=(1-d)^2\boldsymbol{\sigma}_0\quad\text{with}\quad\boldsymbol{\sigma}_0:=\kappa\ \text{tr}[\boldsymbol{\varepsilon}^e]1+2\mu\text{dev}[\boldsymbol{\varepsilon}^e], \tag{79}$$

where $\boldsymbol{\sigma}_0$ to the effective stress tensor dual to the elastic Lagrangian Hencky strain $\boldsymbol{\varepsilon}^e$.

4.3.2. The gradient plastic evolution

The second Euler equation $(66)_2$ of the variational principle (64) determines the PDE for the strain gradient plastic evolution of the equivalent plastic strain. It defines the plastic hardening force in the form

$$r^p = (1-d)^2 r_0^p \quad \text{with} \quad r_0^p := \widehat{y}(\alpha) - y_0 l_p^2 \Delta\alpha \tag{80}$$

in terms of the given *local* hardening function $\widehat{y}$ and the strain gradient term, governed by the Laplacian $\Delta\alpha$ of the equivalent plastic strain. It characterizes a combination of nonlinear local hardening with linear gradient hardening consistent with approaches by Aifantis (1987) and Mühlhaus and Aifantis (1991). The above PDE is accompanied by the Euler equation $(66)_{4,5,6}$ for the evolution equations of the plastic state, which read with the identification of the plastic force $\boldsymbol{f}^p = \mathrm{dev}[\boldsymbol{\sigma}]$ for the von Mises plasticity model

$$\dot{\boldsymbol{\varepsilon}}^p = \lambda^p \frac{\mathrm{dev}[\boldsymbol{\sigma}]}{\|\mathrm{dev}[\boldsymbol{\sigma}]\|} \quad \text{and} \quad \dot{\alpha} = \lambda^p \sqrt{\frac{2}{3}} \tag{81}$$

with the plastic parameter defined by the non-smooth constitutive equation

$$\lambda^p := \frac{3}{2\eta^p} \langle \|\mathrm{dev}[\boldsymbol{\sigma}]\| - \sqrt{\frac{2}{3}} r^p \rangle \tag{82}$$

Note that the degradation function $(1-d)^2$ acts on both the stresses (79) and as well as hardening variable (80). As a consequence, the formulation models a *plastic response in the effective stress space* related to $\boldsymbol{\sigma}_0$ and r_0^p. This response is completely independent of the fracture phase field for a state-dependent choice

$$\eta^p = (1-d)^2 \eta_0^p. \tag{83}$$

of the plastic viscosity. The combination of $(81)_2$ with (82) and (80) results in the PDE for the strain gradient evolution of the hardening variable

$$\dot{\alpha} = \frac{1}{\eta_0^p} \langle \sqrt{\frac{3}{2}} \|\mathrm{dev}[\boldsymbol{\sigma}_0]\| - \left[\widehat{y}(\alpha) - y_0 l_p^2 \Delta\alpha \right] \rangle \tag{84}$$

where the Macauley bracket ensures the irreversibility of the isotropic hardening variable. Clearly, the plastic hardening variable is driven by the equivalent effective stress, and has the typical gradient-type regularization.

4.3.3. The fracture phase field equation

The third Euler equation $(66)_3$ of the variational principle (64) determines the PDE for fracture phase field evolution equation. It defines the fracture driving force

$$f^f - r^f = 2(1-d)\left[\widehat{w}_0^{ep}(\boldsymbol{\varepsilon}^e, \alpha, \nabla\alpha) - w_c \right] - 2\frac{w_c}{\zeta}\left[d - l_f^2 \Delta d \right] \tag{85}$$

in terms of the Laplacian Δd of the crack phase field. The last term contains the variational derivative of the crack surface density function $\gamma(d, \nabla d)$, and can be considered as the crack resistance. The above PDE is accompanied by the Euler equation $(66)_7$ for the evolution of the phase field, which reads

$$\dot{d} = \lambda^f \quad \text{with} \quad \lambda^f := \frac{1}{\eta^f} \langle f^f - r^f \rangle \tag{86}$$

Setting for convenience

$$\eta^f = 2\frac{w_c}{\zeta} \eta_0{}^f, \tag{87}$$

the combination of (86) with (85) characterizes a generalized Ginzburg-Landau- or Allen-Cahn-type equation for the evolution of the crack phase field d

$$\dot{d} = \frac{1}{\eta_0^f} \left\langle (1-d)\zeta \left[\frac{\widehat{w}_0^{ep}}{w_c} - 1 \right] - \left[d - l_f^2 \Delta d \right] \right\rangle \tag{88}$$

where the Macauley bracket ensures the irreversibility of the crack evolution. Clearly, the fracture phase field is driven by the effective elastic–plastic work function $\widehat{w}_0^{ep}$ of the undamaged material. Following the notation of the recent work Miehe et al. (2015), we may recast (88) into

$$\underbrace{\eta_0^f \dot{d}}_{evolution} = \underbrace{(1-d)\mathscr{H}_0}_{crack\ \ force} - \underbrace{\Big[d - l_f^2 \Delta d\Big]}_{crack\ \ resistance} \tag{89}$$

with the maximum value

$$\mathscr{H}_0 = \max_{s\in[0,t]} D_0(\boldsymbol{X}, s) \geq 0 \tag{90}$$

of a dimensionless *crack driving state function*

$$D_0 = \zeta\left\langle \frac{\widehat{w}_0^e(\boldsymbol{\varepsilon}^e)}{w_c} + \frac{\widehat{w}_0^p(\alpha, \nabla\alpha)}{w_c} - 1 \right\rangle \tag{91}$$

obtained in the history of the deformation process. Hence, cracks propagate if the accumulated effective elastic–plastic work density $\widehat{w}_0^{ep}$ exceeds the critical value w_c. This definition has already been proposed by Miehe et al. (2015).

4.4. Possible modifications of the phase field equation

Note that the above definition of the crack driving state function does not differentiate between tension and compression. In order to enforce a brittle crack evolution only in tension, we consider modifications of the crack driving forces as follows.

4.4.1. Modification for fracture in tension

A first variationally consistent approach is based on a modified representation of the work density function introduced in (14)

$$\widehat{W} = \widehat{g}\Big[\widehat{w}_0^{e+} + \widehat{w}_0^p\Big] + \widehat{w}_0^{e-} + (1-\widehat{g})w_c + 2\frac{w_c}{\zeta} l_f \widehat{\gamma} \tag{92}$$

where only a *tensile part* of the stored elastic energy $\widehat{w}_0^{e+}$ degrades due to fracture and the *compression part* $\widehat{w}_0^{e-}$ remains. The decomposition of the elastic work density function (16) into these contributions can be defined by

$$\widehat{w}_0^e = \widehat{w}_0^{e+} + \widehat{w}_0^{e-} \quad \text{with} \quad \widehat{w}_0^{e+}(\boldsymbol{\varepsilon}^e) := \frac{\kappa}{2}\langle \mathrm{tr}[\boldsymbol{\varepsilon}^e]\rangle^2 + \mu \mathrm{tr}\Big[\mathrm{dev}\Big(\boldsymbol{\varepsilon}^{e+}\Big)^2\Big] \tag{93}$$

Here, $\boldsymbol{\varepsilon}^{e+} := \sum_{a=1}^3 \langle \varepsilon_a^e\rangle \boldsymbol{n}_a \otimes \boldsymbol{n}_a$ is the positive elastic strain tensor defined by a spectral decomposition. Note that the definition (93) contains separate positive volumetric and isochoric contributions. As a consequence, the stresses expression (79) takes the modified form

$$\boldsymbol{\sigma} = (1-d)^2 \boldsymbol{\sigma}_0^+ + \boldsymbol{\sigma}_0^- \quad \text{with} \quad \boldsymbol{\sigma}_0^+ := \kappa\langle \mathrm{tr}[\boldsymbol{\varepsilon}^e]\rangle \mathbf{1} + 2\mu \mathrm{dev}\Big[\boldsymbol{\varepsilon}^{e+}\Big]. \tag{94}$$

The variationally consistent crack driving force is obtained by replacing (85) by

$$f^f - r^f = 2(1-d)\Big[\widehat{w}_0^{e+} + \widehat{w}_0^p - w_c\Big] - 2\frac{w_c}{\zeta}\Big[d - l_f^2 \Delta d\Big]. \tag{95}$$

Following the same steps as outlined above, we end up with the modification of the dimensionless crack driving state function (91)

$$D_0 = \zeta\left\langle \frac{\widehat{w}_0^{e+}(\boldsymbol{\varepsilon}^e)}{w_c} + \frac{\widehat{w}_0^p(\alpha, \nabla\alpha)}{w_c} - 1 \right\rangle \tag{96}$$

where the brittle contribution accounts only for the positive elastic energy $\widehat{w}_0^{e+}$.

4.4.2. Stress-based driving force

A further modification can be obtained by replacing the positive elastic strain energy density $\widehat{w}_0^e$ by its dual

$$\widehat{w}_0^{e*}(\boldsymbol{\sigma}_0) = \sup_{\boldsymbol{\varepsilon}^e} \left[\boldsymbol{\sigma}_0 : \boldsymbol{\varepsilon}^e - \widehat{w}_0^e(\boldsymbol{\varepsilon}^e)\right] \tag{97}$$

in the logarithmic stress space. For the quadratic form (16), this results into the closed-form representation of the positive part

$$\widehat{w}_0^{e*+}(\boldsymbol{\sigma}_0) := \frac{1}{2\kappa}\left\langle \frac{1}{3}\mathrm{tr}[\boldsymbol{\sigma}_0]\right\rangle^2 + \frac{1}{4\mu}\mathrm{tr}\left[\mathrm{dev}\left(\boldsymbol{\sigma}_0^+\right)^2\right] \tag{98}$$

dual to $\widehat{w}_0^{e+}$ defined in (93). Here, $\boldsymbol{\sigma}_0^+ := \sum_{a=1}^3 \langle\sigma_{0a}\rangle \boldsymbol{n}_a \otimes \boldsymbol{n}_a$ is the positive logarithmic stress tensor that is for the isotropic response under consideration coaxial to $\boldsymbol{\varepsilon}^{e+}$. For the linear elastic model in the logarithmic strain space the images of $\widehat{w}_0^{e+}$ in (93) and $\widehat{w}_0^{e*+}(\sigma_0)$ in (98) are identical. Hence, the crack driving state function (91) can be expressed

$$D_0 = \zeta\left\langle \frac{\widehat{w}_0^{e*+}(\boldsymbol{\sigma}_0)}{w_c} + \frac{\widehat{w}_0^p(\alpha, \nabla\alpha)}{w_c} - 1\right\rangle \tag{99}$$

in terms of a brittle contribution that depends on the effective stresses $\boldsymbol{\sigma}_0$.

4.4.3. Simplified driving force

An even more simplified driving force, that is *not variational-consistent*, can be obtained by replacing the function (98) by

$$\widehat{\mathfrak{w}}_0^{e*+}(\boldsymbol{\sigma}_0) = \frac{1}{2E}\mathrm{tr}\left[\left(\boldsymbol{\sigma}_0^+\right)^2\right] = \frac{1}{2E}\sum_{a=1}^3 \langle\sigma_{0a}\rangle^2 \tag{100}$$

It is related to a specific elastic work density function $\widehat{w}_0^e$ in (16) with zero Poisson number ν=0, yielding κ=E/3 and μ=E/2. Note that this function characterizes for given $\widehat{\mathfrak{w}}_0^{e*+}$ the *surface of a sphere* in the positive quadrant logarithmic principal stress space. The crack driving state function (89) can be expressed

$$D_0 = \zeta\left\langle \frac{\widehat{\mathfrak{w}}_0^{e*+}(\sigma_0)}{w_c} + \frac{\widehat{w}_0^p(\alpha, \nabla\alpha)}{w_c} - 1\right\rangle \tag{101}$$

in terms of the simplified stress-based brittle contribution.

5. Model investigations I: local homogeneous response

As a first model investigation, features of the proposed framework for coupling elasto-plasticity to damage are demonstrated for a one-dimensional, local and purely homogeneous setting. This provides a conceptual view on the material parameters used.

5.1. Reformulation of constitutive functions for 1D response

Consider a reformulation of the above constitutive functions for a one-dimensional homogeneous response related to ideal plastic conditions without hardening

$$\widehat{W} = \widehat{\psi}^e(\varepsilon - \varepsilon^p, d) + \widehat{D}^{pf}(\alpha, d) \tag{102}$$

with the stored energy and accumulated dissipated work

$$\widehat{\psi}^e = (1-d)^2\frac{E}{2}(\varepsilon - \varepsilon^p)^2 \quad \text{and} \quad \widehat{D}^{pf} = (1-d)^2[y_0\alpha - w_c] + w_c + \frac{w_c}{\zeta}d^2 \tag{103}$$

for a rate-independent response. These functions govern the constitutive expressions for the stress

$$\sigma = \partial_\varepsilon\widehat{\psi}^e = (1-d)^2E(\varepsilon - \varepsilon^p), \tag{104}$$

the driving forces for plasticity and fracture and the associated resistance functions

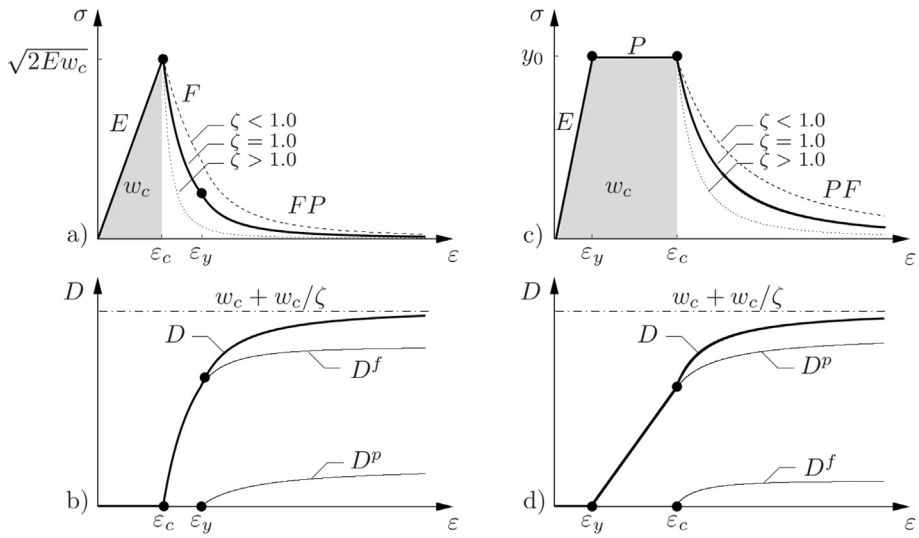

Fig. 4. Stress and Dissipation for Brittle and Ductile Response. Stress σ and dissipated work D for homogeneous test with a–b) *brittle E-F-P response* $\{\varepsilon_c := (2w_c/E)^{1/2}\} < \{\varepsilon_y := y_0/E\}$ and for c–d) *ductile E-P-F response* $\{\varepsilon_c := w_c/y_0 + y_0/2E\} > \{\varepsilon_y := y_0/E\}$. The plastic yield parameter y_0 bounds the effective stress. The fracture threshold parameter w_c determines the onset of fracture and the parameter ζ the shape of the softening due to fracture. The dissipated work $D = D^p + D^f$ contains contributions due to plasticity and fracture and converges to the value $w_c + w_c/\zeta$ at the fully broken state.

$$
\begin{aligned}
f^p &:= -\partial_{\varepsilon^p}\widehat{\psi}^e = (1-d)^2 E(\varepsilon - \varepsilon^p) \\
f^f &:= -\partial_d \widehat{\psi}^e = (1-d)E(\varepsilon - \varepsilon^p)^2 \\
r^p &:= \partial_\alpha \widehat{D}^{pf} = (1-d)^2 y_0 \\
r^f &:= \partial_d \widehat{D}^{pf} = 2(1-d)[w_c - y_0\alpha] + 2w_c d/\zeta
\end{aligned}
\tag{105}
$$

The evolution of the plastic strains and the fracture phase field is governed by the two threshold functions

$$
\widehat{\phi}^p(f^p, r^p) = |f^p| - r^p \quad \text{and} \quad \widehat{\phi}^f\left(f^f - r^f\right) = f^f - r^f. \tag{106}
$$

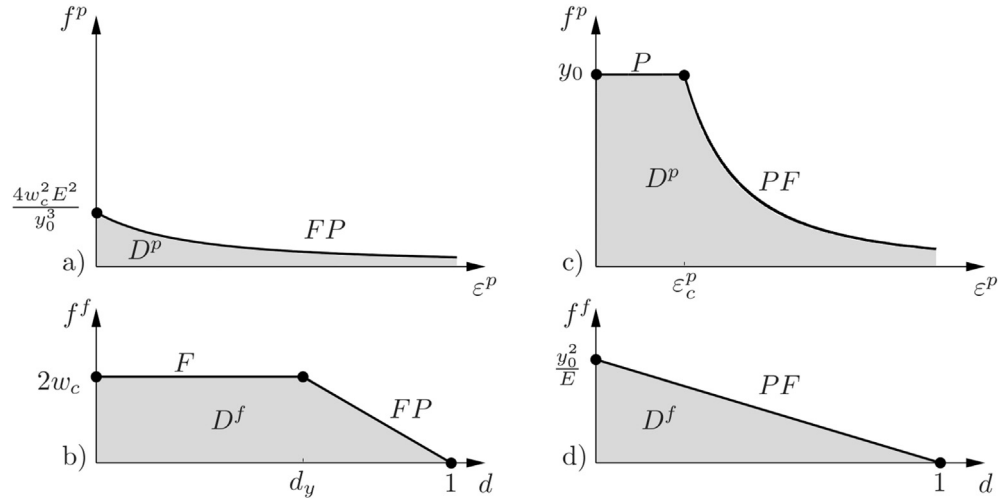

Fig. 5. Driving Forces for Plasticity and Fracture. Qualitative features of the plastic and fracture driving forces f^p and f^f for a–b) *brittle E-F-P response* and for c–d) *ductile E-P-F response*. In brittle fracture, the fracture driving force f^f stays constant up to the onset of plasticity at $d_y = 1 - 2Ew_c/y_0^2$. In ductile fracture, the ideal plastic driving force f^p is constant up to the onset of fracture at $\varepsilon_c^p = w_c/y_0 - y_0/2E$.

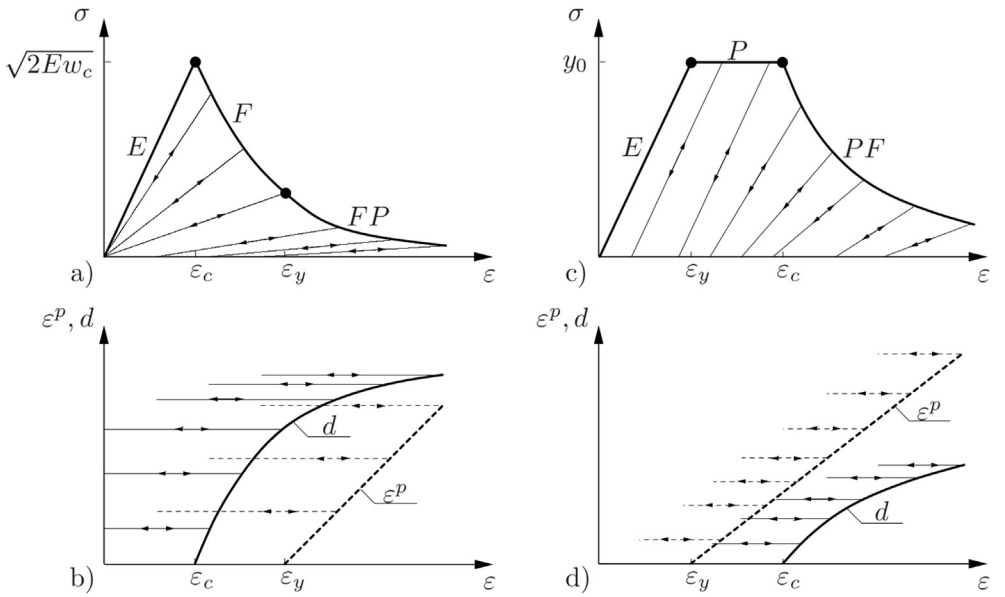

Fig. 6. Loading–Unloading for Brittle and Ductile Response. Qualitative features for a–b) *brittle E-F-P response* and for c–d) *ductile E-P-F response*. The typical brittle damage and ductile plasticity loading-unloading characteristics for the stress superimpose in the post-critical *FP* and *PF* ranges. Plastic strain ε^p and fracture phase field d remain constant during unloading, reflecting the threshold characteristics of the proposed approach.

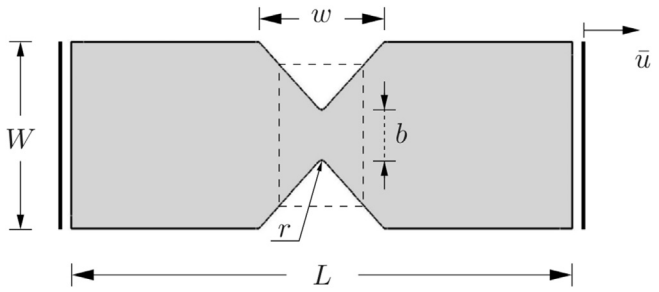

Fig. 7. Plane strain test of V-notch bar in tension. Geometry and boundary conditions.

The response of this one-dimensional model is visualized in Fig. 4. Fig. 5 shows the decomposition of the accumulated dissipative work D into the contributions caused by plasticity and fracture

$$D^p := \int_0^{\varepsilon^p} f^p \, d\tilde{\varepsilon}^p \quad \text{and} \quad D^f := \int_0^{d} f^f \, d\tilde{d} \tag{107}$$

obtained by numerical integration.

Table 1
Material parameters used for the V-notch bar (Al-6061) Li et al (2011).

No.	Parameter	Name	Value	Unit
1.	E	Young's modulus	68.9	GPa
2.	ν	Poisson's ratio	0.33	–
3.	h	Hardening parameter	0.561	GPa
4.	y_0	Initial yield stress	0.475	GPa
5.	w_c	Critical work density	0.18	GPa
6.	η_p	Plastic viscosity	10^{-7}	GPa.s
7.	η_f	Fracture viscosity	10^{-7}	GPa.s
8.	l_p	Plastic length scale	0.6/0.8	mm
9.	l_f	Fracture length scale	0.2/0.3/0.4	mm

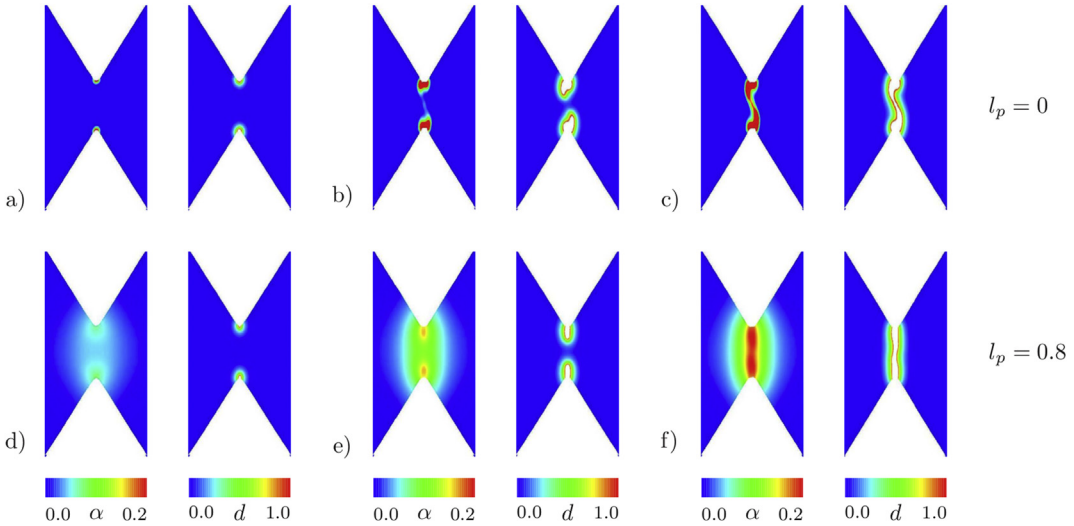

Fig. 8. V-notch bar in tension. Evolution of equivalent plastic strain α and fracture phase field d with two plastic length scales l_p and fixed fracture length scale $l_f = 0.4$ mm. (a)–(c) Local plasticity $l_p = 0$ and (d)–(f) gradient plasticity $l_p = 0.8$ mm for three different stages during deformation up to final failure with crack surfaces related to $d \approx 1$.

5.2. Homogeneous response for brittle and ductile fracture

5.2.1. Brittle fracture

For this one-dimensional scenario, the condition for brittle fracture (55) assumes the simple form

$$\text{Brittle E} - \text{F} - \text{P Response}: \quad w_c < \frac{y_0^2}{2E} \tag{108}$$

the associated onsets of fracture and possible subsequent plasticity are

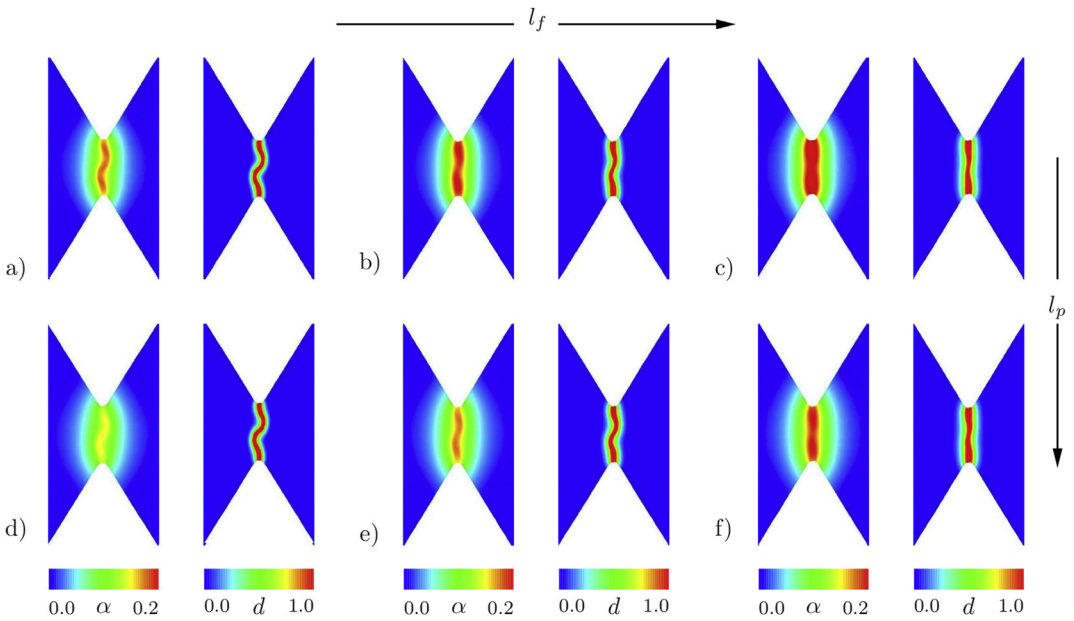

Fig. 9. V-notch bar in tension. Contours of equivalent plastic strain α and fracture phase field d with different combinations of l_f and l_p. a) $l_f = 0.2$ mm, b) $l_f = 0.3$ mm and c) $l_f = 0.4$ mm with $l_p = 0.6$ mm. d) $l_f = 0.2$ mm, e) $l_f = 0.3$ mm and f) $l_f = 0.4$ mm with $l_p = 0.8$ mm.

$$\text{Onset F}: \frac{E}{2}\epsilon^2 = w_c \quad \text{and} \quad \text{Onset P}: \frac{E}{2}\epsilon^2 = \frac{y_0^2}{2E}. \tag{109}$$

These conditions determine a critical strain $\varepsilon{=}\varepsilon_c$, where brittle fracture starts, and a strain $\varepsilon{=}\varepsilon_y$, where a subsequent plastic yielding is initiated. The value of the fracture phase field at the onset of plastic yielding is

$$d = d_y = \frac{y_0^2/E - 2w_c}{y_0^2/E - 2w_c + 2w_c/\zeta} \tag{110}$$

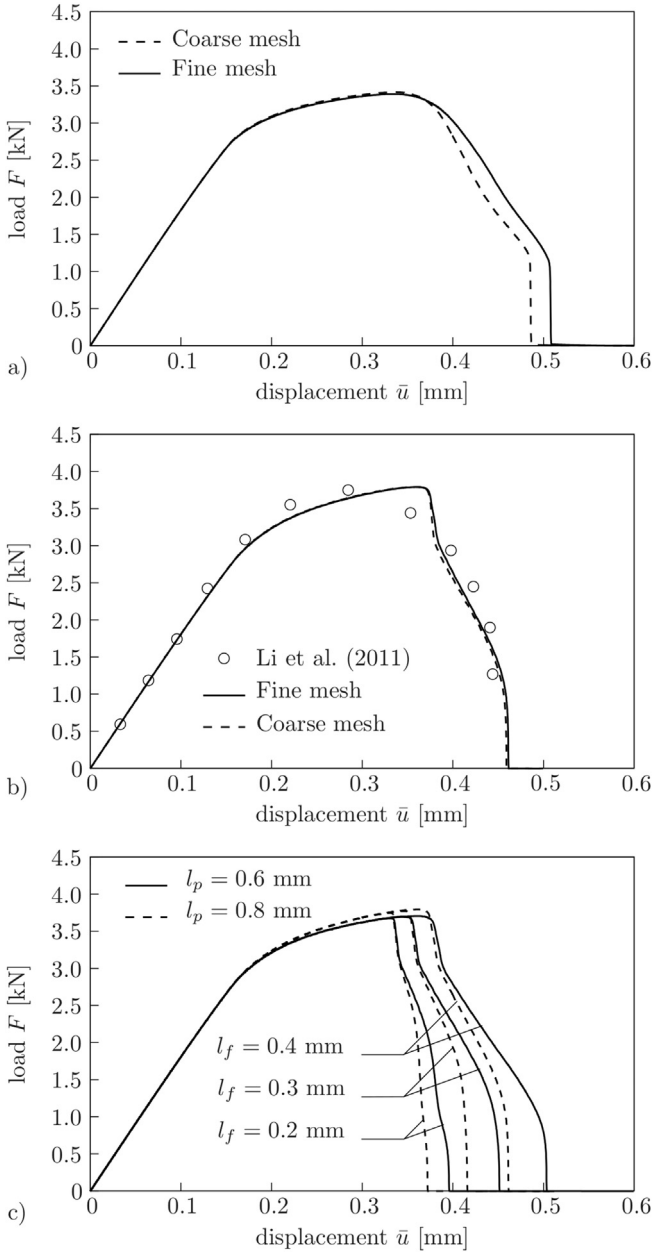

Fig. 10. Load–displacement responses for V-notched bar in tension. a) Mesh sensitivity of local plasticity in the post-critical range for two different mesh discretizations. b) Mesh objectivity of gradient plasticity compared with the data of Li et al. (2011). b) Effects of plastic length scale l_p and the fracture length scale l_f on the overall structural response.

and depends on the material parameter ζ. The visualization in Fig. 5b is performed for the ζ=1, where the crack resistance $r^f = 2w_c$ remains constant before plasticity starts and then decreases linearly $r^f = 2w_c - 2y_0\alpha$ with increasing plastic strain.

Fig. 4a depicts the brittle stress response. Observe that the fracture threshold parameter w_c bounds the elastic response and determines the *onset of fracture*. The shape parameters ζ controls the shape of the post-critical range. It reduces the stress softening due to fracture $\zeta < 1$, where the resistance function $\widehat{D}^{pf}$ is non-convex, and provides more pronounced stress softening due to fracture for $\zeta < 1$, where $\widehat{D}^{pf}$ is non-convex. Fig. 4b reports on the evolution of the dissipated work density D evaluated by numerical integration of the integral expressions (107). Note that D converges to the maximum value $w_c + w_c/\zeta$, which gives an additional meaning to the two material parameters w_c and ζ. Furthermore, observe that the dissipated work D^f due to fracture dominates in this case of brittle fracture, while the subsequently evolving dissipative work D^p due to plasticity is small. These two contributions are also highlighted in Fig. 5a and b, which show the evolutions of the plastic and fracture driving force f^p and f^f, respectively. Note that the fracture driving force f^f remains constant up to the onset of plasticity, and then decreases linearly to zero. Fig. 6a and b characterize the loading-unloading response predicted by the proposed model. It shows initial elastic response E followed by brittle fracture F which unloads till ε_y. Thereafter accumulation of plastic strain with fracture FP is observed.

5.2.2. Ductile fracture

Condition (58) for ductile fracture gives for the one-dimensional model problem

$$\text{Ductile E} - \text{P} - \text{F Response}: \quad w_c > \frac{y_0^2}{2E} \tag{111}$$

with the associated onsets of plasticity and subsequent fracture

$$\text{Onset P}: \frac{E}{2}\varepsilon^2 = \frac{y_0^2}{2E} \quad \text{and} \quad \text{Onset F}: \frac{y_0^2}{2E} + y_0\alpha = w_c. \tag{112}$$

These conditions determine a strain ε=ε_y, where plasticity starts, and a critical equivalent plastic strain α=α_c, where the ductile fracture is initiated. Due to the one-to-one relationship between α_c and w_c, the critical fracture energy is related by

$$w_c = \frac{y_0^2}{2E} + y_0\alpha_c. \tag{113}$$

to a given critical equivalent plastic strain α_c where ductile fracture is initiated.

Fig. 4c shows the ductile response, where the fracture threshold parameter w_c bounds total work density after a considerable amount of plastic deformation. Again the shape parameter ζ determines the slope of the post-critical range of fracture, with $\zeta < 1$ for a convex and $\zeta > 1$ for a non-convex resistance function $\widehat{D}^{pf}$: Fig. 4d shows the evolution of the dissipated work density D up to the limit $w_c + w_c/\zeta$, where now the plastic contribution D^p dominates, successively raising the fracture contribution D^f. The evolution of the dissipative driving forces f^p and f^f for plasticity and fracture are depicted in Fig. 5c and d. Due to the presence of plastic evolution in the full range of fracture, the fracture driving force f^f decreases form the onset of fracture to zero at the fully broken state. The *loading-unloading response* predicted by the proposed model of ductile fracture is visualized in Fig. 6c and d.

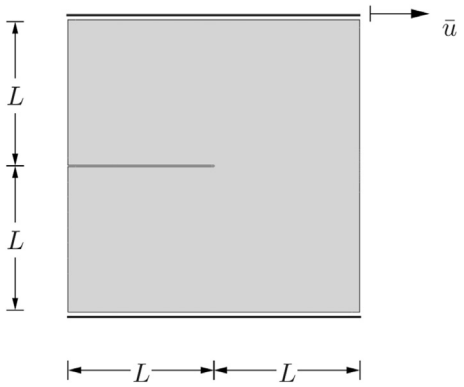

Fig. 11. Single-edge notched shear test. Geometry and boundary conditions.

Table 2
Material parameters used for the single-edge notched shear test.

No.	Parameter	Name	Value	Unit
1.	E	Young's modulus	200	GPa
2.	ν	Poisson's ratio	0.3	–
3.	h	Hardening parameter	0.130	GPa
4.	y_0	Initial yield stress	0.45	GPa
5.	w_c	Critical work density	0.013	GPa
6.	η_p	Plastic viscosity	10^{-7}	GPa.s
7.	η_f	Fracture viscosity	10^{-7}	GPa.s
8.	l_p	Plastic length scale	0.016	mm
9.	l_f	Fracture length scale	0.008	mm

6. Model investigations II: inhomogeneous IBV-Problems

Next, the performance of the proposed phase field model of fracture is demonstrated by means of representative boundary-value problems. Section 6.1 compares the numerical results of the V-notched bar in tension with experimental data of Li et al. (2011). Section 6.2 considers a single-edge notched specimen subjected to shear loading. The key observations of mesh objectivity and physically reasonable interactions of plastic and fracture length scales are highlighted for these two IBVPs. Finally, a three dimensional torsion test of a brittle cast-iron bar and a ductile mild-steel bar is investigated in Section 6.3.

6.1. Analysis of a V-Notch bar in tension test

We model the fracture phenomena of the Al-alloy (Al-6061) of a V-notch bar under tensile loading as reported in the experiments of Li et al. (2011). The aim here is to demonstrate the need for a *gradient extended plasticity coupled with the phase field fracture approach* to overcome the mesh sensitivity in the post-critical range and capture qualitatively the experimentally

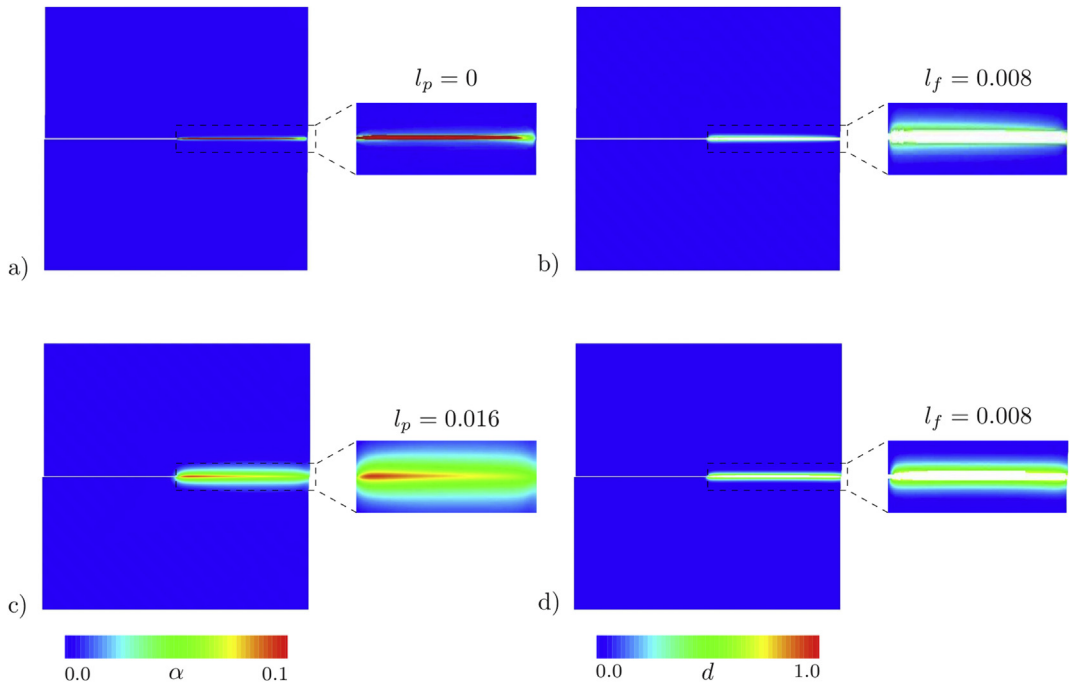

Fig. 12. Single-edge notched shear test. Contour plots of the equivalent plastic strain α and fracture phase field d for two plastic length scales l_p and fixed fracture length scale $l_f = 0.008$ mm. (a)–(b) Local plasticity $l_p = 0$ and (c)–(d) gradient plasticity $l_p = 0.016$ mm at the final deformation state. The crack surfaces are visualized related to $d \approx 1$.

observed load-deflection response. The geometric setup and the loading conditions of the specimen are depicted in Fig. 7. The size of the specimen is chosen to be: $L = 40$ mm, $W = 14$ mm, $b = 4$ mm, $w = 10$ mm, and the radius of the V-notch is $r = 0.25$ mm. The same material parameters are used as in Li et al (2011) and listed in Table 1. The mesh size of the specimen is chosen to be $h_e = 0.1$ mm in the expected fracture zone. The computation is performed by applying the displacement $\overline{u}$ on the right vertical boundary.

The evolution of the crack phase field d compared with the evolution of the equivalent plastic strain α is reported in Fig. 8 for local and gradient plasticity. The contour plots of the local theory with zero plastic length scale parameter $l_p = 0$ and fracture length scale parameter $l_f = 0.4$ mm are shown in Fig. 8a–c. The crack phase field d initiates at the notch tip where the maximum equivalent plastic strain develops, and successively propagates unsymmetrically from the notches inwards till final rupture as an S-shape. Comparing these results with the experimental work of Li et al. (2011), notice first that the *predicted fracture path is not perpendicular to the loading direction* as shown in the experiment. A reason for this effect is the use of the simple von Mises-type isochoric plastic flow. Secondly, we face a *non-physical evolution of the fracture zone outside the plastic zone*.

From the above observations, we conclude the need for a *gradient extended plasticity theory* by introducing the plastic length scale $l_p \geq l_f$ as an additional material parameter in the model. The contour plots of the gradient theory with $l_p = 0.8$ mm and $l_f = 0.4$ mm are shown in Fig. 8d–f. Observe that the failure zone now occurs inside the plastic zone and appears to be perpendicular to the loading direction. Hence, the gradient-plastic regularization provides a spatial smoothing of the plastic, yielding an improved performance of the simple von Mises model in the modeling ductile failure. For visualization of crack surface, deformed regions with a phase field $d \geq c \approx 1$ are not plotted in Fig. 8.

Fig. 9 demonstrates the influence of the plastic length scale l_p and the fracture length scale l_f on the final failure response.

First, the effect of increasing the fracture length scale is investigated by keeping $l_p = 0.6$ mm fixed as shown in Fig. 9a–c. We notice a delayed failure response by increasing l_f, resulting in a fracture path that becomes more perpendicular to the loading direction. Furthermore, the maximum equivalent plastic strain α increases, which is clearly the influence of increased l_f. Next, the effect of an increased plastic length scale $l_p = 0.8$ mm is illustrated in Fig. 9d–f. Observe that the equivalent plastic strain α is smeared out over several elements, thereby reducing the maximum value of α. However, the failure response is similar to Fig. 9a–c.

In order to further emphasize the need of the gradient extended plasticity theory, we illustrate in Fig. 10 the load-deflection curves of the overall structural response. The mesh sensitivity in the post-critical range observed in local

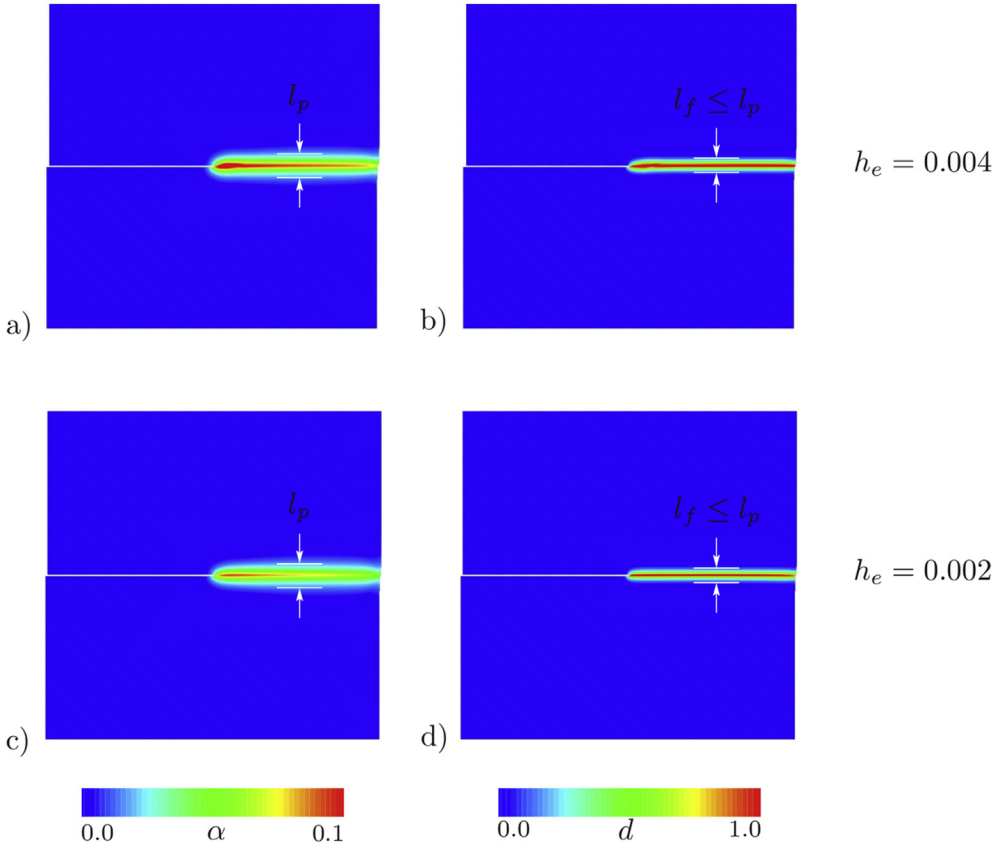

Fig. 13. Single-edge notched shear test. Contour plots of the equivalent plastic strain α (a)–(c) and the fracture phase field d (b)–(d) for two different mesh discretizations at the final deformation state to demonstrate the mesh objectivity of gradient plasticity.

plasticity is shown in Fig. 10a for two different discretizations. To overcome this behavior, gradient plasticity with plastic length scale $l_p = 0.8$ mm is used in Fig. 10b, where mesh objectivity is obtained. Furthermore, observe that the results of the gradient extended plasticity are in qualitative agreement with the experimental results of Li et al. (2011) for both the coarse as well as the fine mesh. Finally, Fig. 10c demonstrates the influence of the fracture length scale l_f and the plastic length scale l_p on the load–deflection response, which corresponds to the analysis in Fig. 9. We observe a delayed-failure response by increasing the fracture length scale and a slightly more pronounced hardening by increasing the plastic length scale.

6.2. Investigation of single-edge notched shear test

The second benchmark test considers a square plate with a horizontal notch placed at the middle height from the left outer surface to the center of the specimen. The geometric setup and the loading conditions of the specimen are depicted in Fig. 11. The size of the square specimen is chosen to be $L = 0.5$ mm. We fixed the bottom edge of the plate and applied shear loading to

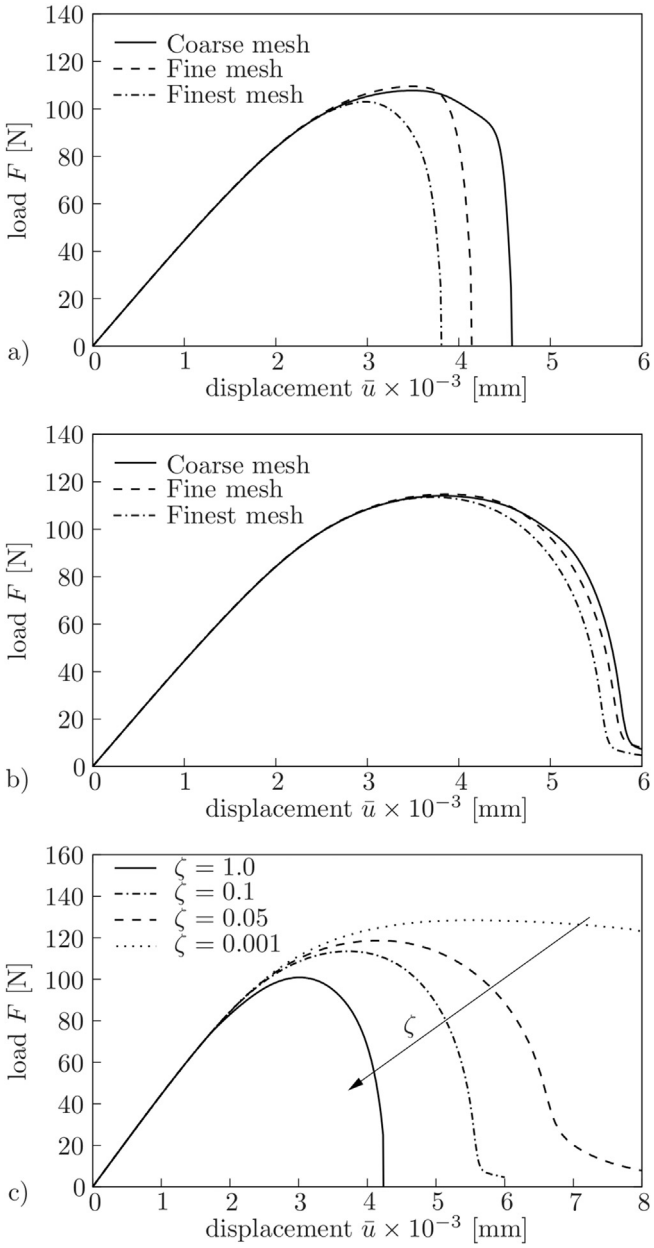

Fig. 14. Load–displacement responses for single-edge notched shear test. a) Mesh sensitivity of local plasticity model in the post-critical range and b) mesh objectivity of the gradient plasticity model for three different mesh discretizations. c) Effects of four different fracture parameters ζ on the crack initiation and load–displacement response.

Table 3
Material parameters used for the torsion test of mild-steel bar.

No.	Parameter	Name	Value	Unit
1.	E	Young's modulus	200	GPa
2.	ν	Poisson's ratio	0.3	–
3.	h	Hardening parameter	0.2	GPa
4.	y_0	Initial yield stress	0.45	GPa
5.	y_∞	Infinite yield stress	0.6	GPa
6.	η	Saturation parameter	16.96	–
7.	w_c	Critical work density	0.04	GPa
8.	η_p	Plastic viscosity	10^{-7}	GPa.s
9.	η_f	Fracture viscosity	10^{-7}	GPa.s
10.	l_p	Plastic length scale	1.4	mm
11.	l_f	Fracture length scale	1.0	mm

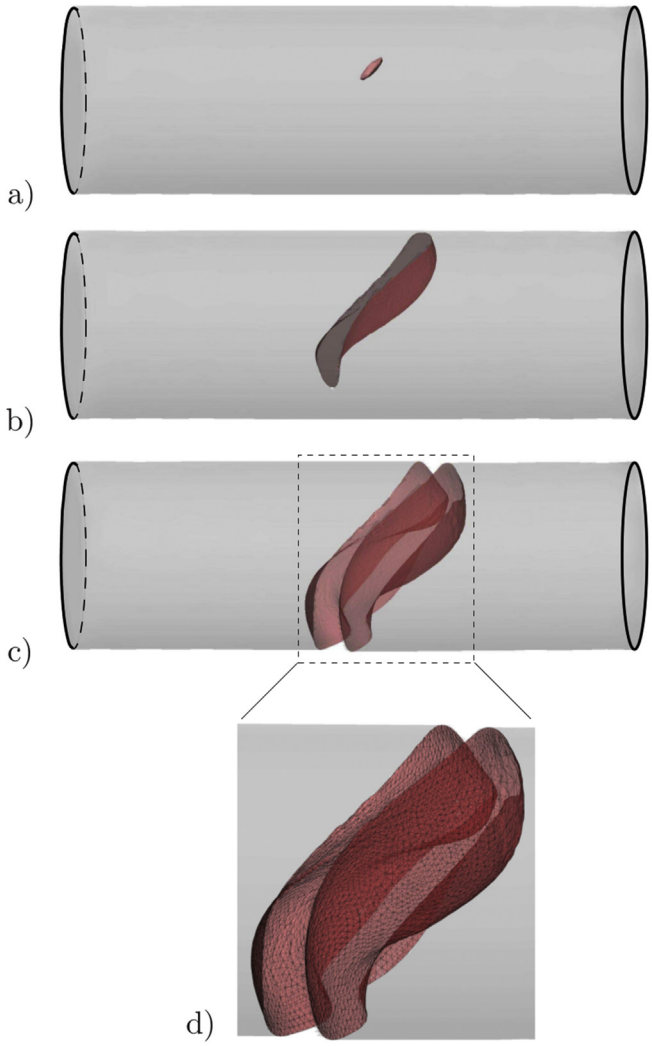

Fig. 15. Three-dimensional torsion test of a circular bar. a)–c) Fracture phase field d evolution in *brittle cast-iron* test for a twist loading. d) Visualization of the crack faces.

the top edge where the vertical displacement is fixed. The material parameters used are given in Table 2. The specimen is discretized by using three different meshes with the maximum element size of $h_e = 0.004$ mm in the expected fracture zone.

The contour plots of the equivalent plastic strain α and the fracture phase field d for local and gradient plasticity with fixed fracture length scale $l_f = 0.008$ mm are plotted in Fig. 12. For local plasticity, observe the non-physical evolution of the fracture zone outside the plastic zone as demonstrated in Fig. 12a–b. The mesh sensitivity in the post-critical response with local plasticity is shown in Fig. 14a for three different meshes.

To overcome this behavior, gradient plasticity with plastic length scale $l_p = 0.016$ mm is used, resulting in a fracture zone to be *inside the plastic zone*. Furthermore, the equivalent plastic strain is smeared over several elements as shown in Fig. 12c–d. Fig. 13 demonstrate the mesh objectivity of the gradient theory for the coarse and finest mesh discretizations. Observe that α and d are almost the same for all the meshes. The corresponding load–displacement curves for the three meshes are shown in Fig. 14b, where the post-critical softening response provides approximately a mesh-objective behavior.

To illustrate the *influence of the fracture parameter* ζ on the crack initiation and propagation, Fig. 14c plots the load–displacement response for four different values of ζ. One observes the expected delayed failure behavior by decreasing the value of ζ.

6.3. Three dimensional torsion test of a cylindrical bar

The last model problem is concerned with analyzing brittle fracture of cast-iron and ductile fracture of mild-steel bars under torsional loading. The purpose of this test is to illustrate the effects on the crack initiation and propagation. We

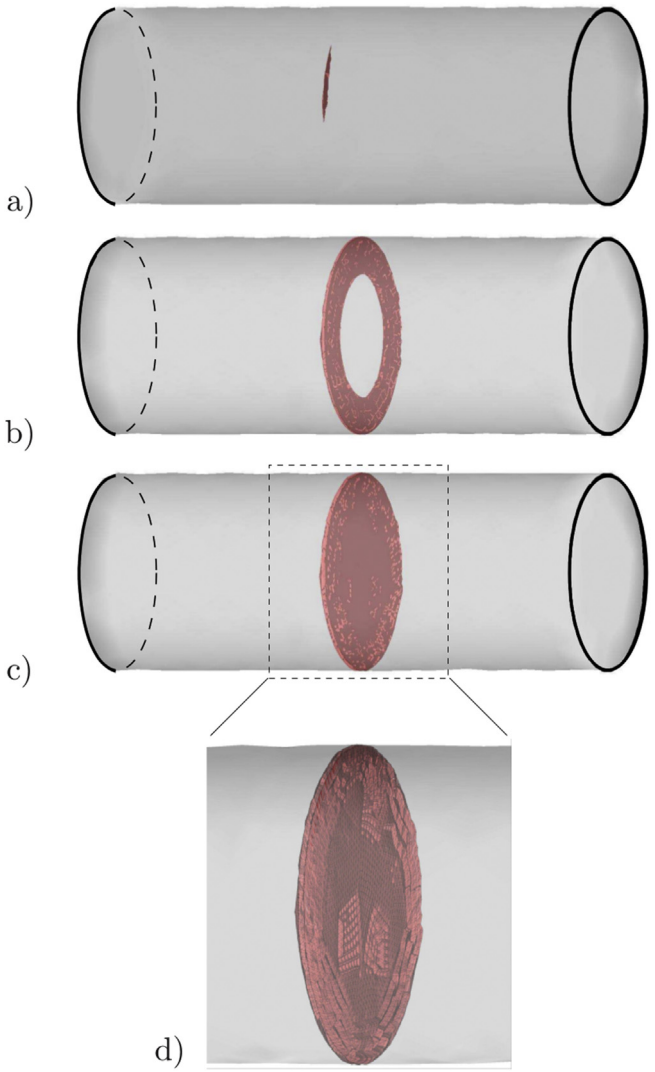

Fig. 16. Three-dimensional torsion test of a circular bar. a)–c) Fracture phase field d evolution in *ductile mild-steel* test for a twist loading. d) Visualization of the crack faces.

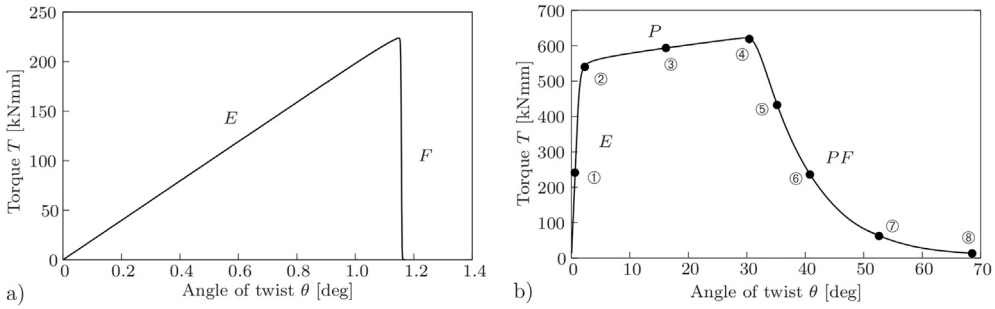

Fig. 17. Torque versus angle of twist for three dimensional torsion test of a circular bar. a) *Brittle failure* of cast-iron bar and b) *Ductile failure* of mild-steel bar.

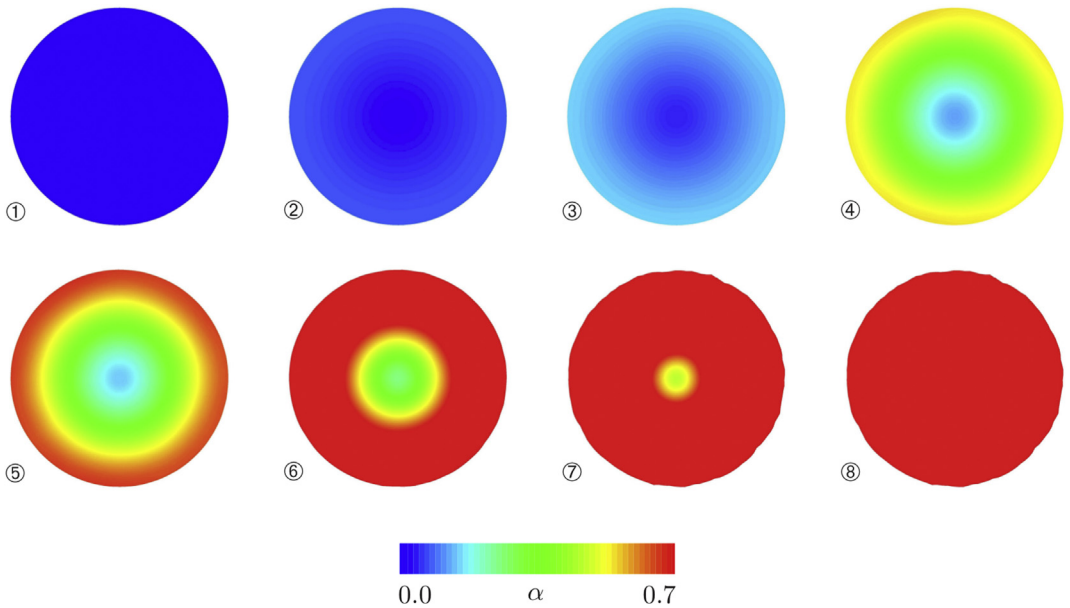

Fig. 18. Torsion test of a ductile circular bar. 1–8 Equivalent plastic strain α evolution of ductile mild-steel in the cross section near the center of the bar for a twist loading corresponding to the torque T versus angle of twist θ plotted in Fig. 17b.

differentiate between two cases: *brittle fracture* (elastic-fracture) and *ductile fracture* (elastic-plastic-fracture). As a geometric setup, the length of the cylindrical bar is chosen to be $L = 60$ mm and the radius $R = 10$ mm. The computation is performed by fixing one end of the cylindrical bar and applying torsion to the other end. For *brittle cast-iron*, Young's modulus is chosen to be $E = 110$ GPa, Poisson's ratio is set to ν=0.3, the fracture length scale $l_f = 1.0$ mm, and the critical work density to $w_c = 0.1$ MPa. For *ductile mild-steel*, the material parameters used are listed in Table 3. The specimens are discretized with a mesh size of $h_e = l_f/2$ in the expected fracture zone. The evolution of the crack phase field d for the cast-iron and mild-steel bars are depicted in Figs. 15 and 16, respectively.

For the *brittle failure* of cast-iron bar, the crack starts to initiate at a point on the surface near the center of the specimen at an angle of twist of 1.1°, see Fig. 15a. The crack then propagates from the surface inwards till final rupture in Fig. 15c. To illustrate the crack surface, we zoomed out the fractured area as shown in Fig. 15d. Since the fracture path is about 45° from the longitudinal direction, the fracture surface is complicated and looks like a *helicoid* as plotted in Fig. 15c, where we used a transparency effect to show the failure surface for $d \geq c \approx 1$.

The torsion test is repeated for the *ductile failure* of mild-steel. An inhomogeneous plastic zone develops as a consequence of an initial imperfection at a point on the central surface. The amplitude of this imperfection is sufficiently small such that it does not affect the overall structural response. Fig. 16a depicts the crack initiation on the surface near the center of the bar at about 30° angle of twist. The crack then propagates from the surface inwards perpendicular to the longitudinal direction as shown in Fig. 16c. A zoom of the crack surfaces is shown in Fig. 16d.

The torque T versus angle of twist θ for the overall structural response are illustrated in Fig. 17. The angle of twist θ is measured at the end of the cylindrical bar. For *brittle fracture*, the material response corresponds to the sequence: E(elastic) - F(fracture) plotted in Fig. 17a. Here, the local fracture evolution starts when the elastic energy reaches a critical value w_c. Thereafter, a brittle failure response is observed. For *ductile fracture*, the structural response corresponds to the sequence:

E(elastic) − P(plastic) − FP(fracture−plastic) as shown in Fig. 17b, where the crack phase field is driven by the coupled elastic−plastic driving force (96). The evolution of the equivalent plastic strain α at the center of the bar, corresponding to Fig. 17b, is plotted for different stages of deformation up to final failure as in Fig. 18. α starts to evolve after initial yielding, see Fig. 18 2−3, thereafter fracture starts at 4. Observe that the equivalent plastic strain is increasing from the surface to the center of the specimen as illustrated in Fig. 18 5−8, which corresponds with the fracture phase field d depicted in Fig. 16c.

7. Conclusion

A variational-based framework for the phase field modeling of ductile fracture in elastic−plastic solids undergoing large strains was proposed. The phase field approach regularizes sharp crack surfaces within a pure continuum setting by a specific gradient damage modeling with constitutive terms rooted in fracture mechanics. It was linked to a formulation of gradient plasticity at finite strains. As a consequence, that formulation includes two independent length scales which regularize both the plastic response as well as the crack discontinuities. This ensures that the damage zones of ductile fracture are inside of plastic zones, and guarantees on the computational side a mesh objectivity in post-critical ranges. An important novel aspect of this work was a precise representation of this framework based on a canonical minimization principle. The coupling of gradient plasticity to gradient damage was realized by a constitutive work density function that includes the stored elastic energy and the dissipated work due to plasticity and fracture. The latter represents a coupled resistance to plasticity and damage, depending on the gradient-extended internal variables which enter plastic yield functions and fracture threshold functions. The thermodynamic consistent formulation was outlined for gradient-extended dissipative solids in terms of generalized internal variables which are passive in nature. This canonical theory proposed is shown to be governed by a rate-type minimization principle, which fully determines the coupled multi-field evolution problem. This is exploited on the numerical side by a fully symmetric monolithic finite element implementation. The performance of the formulation was demonstrated by means of representative examples.

Acknowledgment

Support for this research was provided by the German Research Foundation (DFG) within the Cluster of Excellence Exc 310 *Simulation Technology* at the University of Stuttgart.

References

Aifantis, E.C., 1987. The physics of plastic deformation. Int. J. Plast. 3, 211−247.
Alessi, R., Marigo, J.-J., Vidoli, S., 2015. Gradient damage models coupled with plasticity: variational formulation and main properties. Mech. Mater. 80, 351−367.
Ambati, M., Gerasimov, T., De Lorenzis, L., 2015. Phase-field modeling of ductile fracture. Comput. Mech. 55, 1017−1040.
Ambrosio, L., Tortorelli, V.M., 1990. Approximation of functionals depending on jumps by elliptic functionals via Γ-convergence. Commun. Pure Appl. Math. 43, 999−1036.
Anand, L., 1979. On h. hencky's approximate strain-energy function for moderate deformations. J. Appl. Mech. 46, 78−82.
Aslan, O., Cordero, N., Gaubert, A., Forest, S., 2011. Micromorphic approach to single crystal plasticity and damage. Int. J. Eng. Sci. 49, 1311−1325.
Belytschko, T., Black, T., 1999. Elastic crack growth in finite elements with minimal remeshing. Int. J. Numer. Methods Eng. 45, 601−620.
Besson, J., 2010. Continuum models of ductile fracture: a review. Int. J. Damage Mech. 19, 3−52.
Borden, M.J., Verhoosel, C.V., Scott, M.A., Hughes, T.J.R., Landis, C.M., 2012. A phase-field description of dynamic brittle fracture. Comput. Methods Appl. Mech. Eng. 217−220, 77−95.
Borden, M.J., Hughes, T.J.R., Landis, C.M., Verhoosel, C.V., 2014. A higher-order phase-field model for brittle fracture: formulation and analysis within the isogeometric analysis framework. Comput. Methods Appl. Mech. Eng. 273, 100−118.
Bourdin, B., Francfort, G.A., Marigo, J.J., 2000. Numerical experiments in revisited brittle fracture. J. Mech. Phys. Solids 48, 797−826.
Bourdin, B., Francfort, G., Marigo, J.-J., 2008. The Variational Approach to Fracture. Springer.
Brünig, M., Gerke, S., Hagenbrock, V., 2013. Micro-mechanical studies on the effect of the stress triaxiality and the lode parameter on ductile damage. Int. J. Plast. 50, 49−65.
Capriz, G., 1989. Continua with Microstructure. Springer.
Clayton, J., 2011. Nonlinear Mechanics of Crystals. Springer, Dordrecht.
Comi, C., 1999. Computational modelling of gradient-enhanced damage in quasi-brittle materials. Mech. Cohesive-frictional Mater. 4, 17−36.
Crete, J., Longere, P., Cadoua, J., 2014. Numerical modelling of crack propagation in ductile materials combining the gtn model and x-fem. Comput. Methods Appl. Mech. Eng. 275, 204−233.
Danas, K., Ponte Castañeda, P., 2012. Influence of the lode parameter and the stress triaxiality on the failure of elasto-plastic porous materials. Int. J. Solids Struct. 49, 1325−1342.
de Borst, R., Pamin, J., Geers, M.G.D., 1999. On coupled gradient-dependent plasticity and damage theories with a view to localization analysis. Eur. J. Mech. A/Solids 18, 939−962.
Dimitrijevic, B.J., Hackl, K., 2011. A regularization framework for damage-plasticity models via gradient enhancement of the free energy. Int. J. Numer. Methods Biomed. Eng. 27, 1199−1210.
Duda, F.P., Ciarbonetti, A., sánchez, P.J., Huespe, A.E., 2014. A phase-field/gradient damage model for brittle fracture in elastic-plastic solids. Int. J. Plast. 65, 269−296.
Evers, L.P., Brekelmans, W.A.M., Geers, M.G.D., 2004. Scale dependent crystal plasticity framework with dislocation density and grain boundary effects. Int. J. Solids Struct. 41, 5209−5230.
Fleck, N.A., Hutchinson, J.W., 1997. Strain gradient plasticity. Adv. Appl. Mech. 33, 295−362.
Forest, S., 2009. Micromorphic approach for gradient elasticity, viscoplasticity, and damage. J. Eng. Mech. 135, 117−131.
Francfort, G.A., Marigo, J.J., 1998. Revisiting brittle fracture as an energy minimization problem. J. Mech. Phys. Solids 46, 1319−1342.
Frémond, M., 2002. Non-smooth Thermomechanics. Springer.
Frémond, M., Nedjar, B., 1996. Damage, gradient of damage, and principle of virtual power. Int. J. Solids Struct. 33, 1083−1103.

Geers, M.G.D., 2004. Finite strain logarithmic hyperelasto-plasticity with softening: a strongly non-local implicit gradient framework. Comput. Methods Appl. Mech. Eng. 193, 3377–3401.
Gurson, A.L., 1975. Continuum Theory of Ductile Rupture by Void Nucleation and Growth. Part I – Yield Criteria and Flow Rules for Porous Ductile Media. Division of Engineering, Brown University.
Gurtin, M.E., 1996. Generalized ginzburg-landau and cahn-hilliard equations based on a microforce balance. Phys. D Nonlinear Phenom. 92, 178–192.
Gurtin, M.E., 2002. A gradient theory of single-crystal viscoplasticity that accounts for geometrically necessary dislocations. J. Mech. Phys. Solids 50, 5–32.
Gurtin, M.E., 2003. On a framework for small-deformation viscoplasticity: free energy, microforces, strain gradients. Int. J. Plast. 19, 47–90.
Hakim, V., Karma, A., 2009. Laws of crack motion and phase-field models of fracture. J. Mech. Phys. Solids 57, 342–368.
Hofacker, M., Miehe, C., 2012. Continuum phase field modeling of dynamic fracture: variational principles and staggered fe implementation. Int. J. Fract. 1–17.
Huespe, A., Needleman, A., Oliver, J., Sánchez, 2009. A finite thickness band method for ductile fracture analysis. Int. J. Plast. 25, 2349–2365.
Huespe, A., Needleman, A., Oliver, J., Sánchez, 2012. A finite strain, finite band method for modeling ductile fracture. Int. J. Plast. 28, 53–69.
Johnson, G., Cook, W., 1985. Fracture characteristics of three metals subjected to various strains, strain rates, temperatures and pressures. Eng. Fract. Mech. 21, 31–48.
Karma, A., Kessler, D.A., Levine, H., 2001. Phase-field model of mode III dynamic fracture. Phys. Rev. Lett. 87, 045501.
Khan, A., Liu, H., 2012. A new approach for ductile fracture prediction on al 2024-t351 alloy. Int. J. Plast. 35, 1–12.
Kröner, E., 1960. Allgemeine Kontinuumstheorie der Versetzungen und Eigenspannungen. Arch. Ration. Mech. Anal. 4, 273–334.
Leblond, J., Perrin, G., Suquet, P., 1994. Exact results and approximate models for porous viscoplastic solids. Int. J. Plast. 3, 213–235.
Lemaitre, J., 1985. A continuous damage mechanics model for ductile fracture. J. Eng. Mater. Technol. 107, 83–89.
Lemaitre, J., Chaboche, J., 1990. Mechanics of Solid Materials. Cambridge University Press.
Li, H., Fu, M., Lu, J., Yang, H., 2011. Ductile fracture: experiments and computations. Int. J. Plast. 27, 147–180.
Linder, C., Raina, A., 2013. A strong discontinuity approach on multiple levels to model solids at failure. Comput. Methods Appl. Mech. Eng. 253, 558–583.
Mariano, P.M., 2001. Multifield theories in mechanics of solids. Adv. Appl. Mech. 38, 1–93.
Maugin, G.A., 1990. Internal variables and dissipative structures. J. Non-Equilib. Thermodyn. 15, 173–192.
Miehe, C., 1998. A constitutive frame of elastoplasticity at large strains based on the notion of a plastic metric. Int. J. Solids Struct. 35, 3859–3897.
Miehe, C., 2011. A multi-field incremental variational framework for gradient-extended standard dissipative solids. J. Mech. Phys. Solids 59, 898–923.
Miehe, C., 2014. Variational gradient plasticity at finite strains. Part I: mixed potentials for the evolution and update problems of gradient-extended dissipative solids. Comput. Methods Appl. Mech. Eng. 268, 677–703.
Miehe, C., Gürses, E., 2007. A robust algorithm for configurational-force-driven brittle crack propagation with r-adaptive mesh alignment. Int. J. Numer. Methods Eng. 72, 127–155.
Miehe, C., Apel, N., Lambrecht, M., 2002. Anisotropic additive plasticity in the logarithmic strain space. Modular kinematic formulation and implementation based on incremental minimization principles for standard materials. Comput. Methods Appl. Mech. Eng. 191, 5383–5425.
Miehe, C., Welschinger, F., Hofacker, M., 2010. Thermodynamically consistent phase-field models of fracture: variational principles and multi-field fe implementations. Int. J. Numer. Methods Eng. 83, 1273–1311.
Miehe, C., Hofacker, M., Welschinger, F., 2010. A phase field model for rate-independent crack propagation: robust algorithmic implementation based on operator splits. Comput. Methods Appl. Mech. Eng. 199, 2765–2778.
Miehe, C., Aldakheel, F., Mauthe, S., 2013. Mixed variational principles and robust finite element implementations of gradient plasticity at small strains. Int. J. Numer. Methods Eng. 94, 1037–1074.
Miehe, C., Welschinger, F., Aldakheel, F., 2014. Variational gradient plasticity at finite strains. Part II: local-global updates and mixed finite elements for additive plasticity in the logarithmic strain space. Comput. Methods Appl. Mech. Eng. 268, 704–734.
Miehe, C., Hofacker, M., Schänzel, L.-M., Aldakheel, F., 2015. Phase field modeling of fracture in multi-physics problems. Part II. brittle-to-ductile failure mode transition and crack propagation in thermo-elastic-plastic solids. Comput. Methods Appl. Mech. Eng. 294, 486–522.
Moës, N., Dolbow, J., Belytschko, T., 1999. A finite element method for crack growth without remeshing. Int. J. Numer. Methods Eng. 46, 131–150.
Mühlhaus, H.-B., Aifantis, E.C., 1991. A variational principle for gradient plasticity. Int. J. Solids Struct. 28, 845–857.
Mumford, D., Shah, J., 1989. Optimal approximations by piecewise smooth functions and associated variational problems. Commun. Pure Appl. Math. 42, 577–685.
Nahshon, K., Hutchinson, J., 2008. Modification of the gurson model for shear failure. Eur. J. Mech. A/Solids 27, 1–17.
Nedjar, B., 2001. Elastoplastic-damage modelling including the gradient of damage: formulation and computational aspects. Int. J. Solids Struct. 38, 5421–5451.
Needleman, A., Tvergaard, V., 1984. An analysis of ductile rupture in notched bars. J. Mech. Phys. Solids 32, 461–490.
Nye, J.F., 1953. Some geometrical relations in dislocated crystals. Acta Metall. 1, 153–162.
Oliver, J., 1996a. Modelling strong discontinuities in solid mechanics via strain softening constitutive equations. Part1: fundamentals. Int. J. Numer. Methods Eng. 39, 3575–3600.
Oliver, J., 1996b. Modelling strong discontinuities in solid mechanics via strain softening constitutive equations. Part2: numerical simulation. Int. J. Numer. Methods Eng. 39, 3601–3623.
Ortiz, M., Pandolfi, A., 1999. Finite-deformation irreversible cohesive elements for three-dimensional crack-propagation analysis. Int. J. Numer. Methods Eng. 44, 1267–1282.
Peerlings, R.H.J., de Borst, R., Brekelmans, W.A.M., de Vree, J.H.P., 1996. Gradient enhanced damage for quasi–brittle materials. Int. J. Numer. Methods Eng. 39, 3391–3403.
Pham, K., Amor, H., Marigo, J., Maurini, C., 2011. Gradient damage models and their use to approximate brittle fracture. Int. J. Damage Mech. 20, 618–652.
Ponte Castañeda, P., Zaidman, M., 1994. Constitutive models for porous materials with evolving microstructure. J. Mech. Phys. Solids 42, 1459–1497.
Reddy, B., Ebobisse, F., McBride, A., 2008. Well-posedness of a model of strain gradient plasticity for plastically irrotational materials. Int. J. Plast. 24, 55–73.
Reusch, F., Svendsen, B., Klingbeil, D., 2003. Local and non-local gurson-based ductile damage and failure modelling at large deformation. Eur. J. Mech. A/Solids 22, 779–792.
Rice, J.R., Tracey, D.M., 1969. On the ductile enlargement of voids in triaxial stress fields. J. Mech. Phys. Solids 17, 201–217.
Saanouni, K., Hamed, M., 2013. Micromorphic approach for finite gradient-elastoplasticity fully coupled with ductile damage: formulation and computational aspects. Int. J. Solids Struct. 50, 2289–2309.
Simo, J.C., Oliver, J., Armero, F., 1993. An analysis of strong discontinuities induced by strain-softening in rate-independent inelastic solids. Comput. Mech. 12, 277–296.
Steinmann, P., 2015. Geometrical Foundations of Continuum Mechanics. Springer, Berlin.
Svendsen, B., 2002. Continuum thermodynamic models for crystal plasticity including the effects of geometrically-necessary dislocations. J. Mech. Phys. Solids 50, 1297–1329.
Ulmer, H., Hofacker, M., Miehe, C., 2013. Phase field modeling of brittle and ductile fracture. Proc. Appl. Math. Mech. 13, 533–536.
Verhoosel, C.V., de Borst, R., 2013. A phase-field model for cohesive fracture. Int. J. Numer. Methods Eng. 96, 43–62.
Wells, G.N., Sluys, L.J., 2001. A new method for modelling cohesive cracks using finite elements. Int. J. Numer. Methods Eng. 50, 2667–2682.
Xu, X.P., Needleman, A., 1994. Numerical simulations of fast crack growth in brittle solids. J. Mech. Phys. Solids 42, 1397–1434.